Supplementary Materials

Identification of nuclear pore proteins at plasmodesmata

T. Moritz Schladt[1,2,*], Manuel Miras[1,2,8,*], Jona Obinna Ejike[1,2,*], Mathieu Pottier[1,2,9,*], Lin Xi[3], Andrea Restrepo-Escobar[1,2], Masayoshi Nakamura[4], Niklas Pütz[1,2], Sebastian Hänsch[2,5], Julia Engelhorn[1,2], Chen Gao[1,2], Marcel Dickmanns[1,2,6], Gwendolyn V. Davis[1,2], Ahan Dalal[1,2], Sven Gombos[3], Ronja Lange[1,2], Rüdiger Simon[2,7], Waltraud X. Schulze[3] & Wolf B. Frommer[1,2,4,§]

[1] Heinrich Heine University Düsseldorf, Faculty of Mathematics and Natural Sciences, Institute for Molecular Physiology, Düsseldorf, Germany
[2] Cluster of Excellence on Plant Sciences, Heinrich Heine University Düsseldorf, Germany
[3] Department of Plant Systems Biology, University of Hohenheim, 70593 Stuttgart, Germany
[4] Institute for Transformative Biomolecules (WPI-ITbM), Nagoya University, Nagoya, Japan
[5] Center for Advanced Imaging; Heinrich Heine University Düsseldorf, Düsseldorf, Germany
[6] Department of Molecular Structural Biology, Max Planck Institute of Biochemistry, Martinsried, Germany
[7] Heinrich Heine University Düsseldorf, Faculty of Mathematics and Natural Sciences, Institute of Developmental Genetics, Germany
[8] New address: Department of Stress Biology and Plant Pathology, CEBAS-CSIC, Murcia, Spain
[9] New address: Université de Lorraine, INRAE, IAM, F-54000 Nancy, France

* Equal contribution
§ For correspondence: frommew@hhu.de

Materials and Methods

Plant materials and growth conditions

Physcomitrium patens (*P. patens*) ecotype Grandsen cultures were obtained from the *International Moss Stock Center (IMSC)* (Freiburg). *P. patens* was cultured in liquid cultures of modified BCD medium as described [1]. The BCD medium consisted of the following solutions which were mixed prior to use: Solution B (0.1 mM $MgSO_4 \cdot 7H_2O$), Solution C (1.84 mM KH_2PO_4), Solution DK (1 M KNO_3), Solution DF (4.5 mM $FeSO_4 \cdot 7H_2O$), Trace Element Solution (TES) (614 mg H_3BO_3, 55 mg $CuSO_4 \cdot 5H_20$, 28 mg KBr, 110 mg $Al_2(SO_4)3 \cdot K_2SO_4 \cdot 24H_20$, 389 mg $MnCl_2 \cdot 4H_20$, 55 mg $ZnSO_4 \cdot 7H_20$, 28mg LiCl, 10 mM $CoCl_2 \cdot 6H_20$, 28 mg KI and 28 mg $SnCl_2 \cdot 2H_20$ in 1 L H_20), 500 mM diammonium tartrate and 1 M $CaCl_2$. For liquid cultures, 1% (m/v) glucose was added. For propagation of liquid cultures, moss was homogenized and then transferred to 100 ml medium in a 250 ml. Cultures were harvested after two weeks of growth at 21°C under long day conditions (16 h light/8 h dark) at ~90 µmol m^{-2} sec^{-1}, 60% humidity.

Arabidopsis *cpr5-1* (G420D) mutant and *cpr5-T3* (SALK_074631) T-DNA insertion mutant were kindly provided by Dr. Gu (University of California Berkeley) and Professor Chun-Hai Dong (Qingdao Agricultural University), respectively [2,3]. Arabidopsis *NUP62-1* (SALK_079143) and *NUP62-2* (SALK_037337) T-DNA insertion mutant were obtained from the Nottingham Arabidopsis Stock Centre (NASC). Arabidopsis Col-0 *shr*/pSHR:SHR–GFP line was described before [4] and kindly gifted by Ikram Blilou, KAUST. The pSHR:SHR–GFP/*cpr5-1* in the *shr* mutant background was generated by crossing, and identified in the F2 segregating generation by sequencing of CPR5. For quantification of the SHR-GFP endodermis-to-stele ratio, F5 seedlings of the Arabidopsis lines pSHR:SHR–GFP *cpr5-1* were grown on a glass plate coated with ½ Murashige and Skoog (MS) media agar [half-strength Murashige and Skoog basal salt mixture (Duchefa Biochemie, Haarlem, The Netherlands), 0.1 % (w/v) 2-(N-morpholino)-ethanesulfonic acid, 1.5% agar, pH 5.6] [5] for 6 days in short day conditions (10 h light, 14 h darkness), at 21°C with a light intensity to 130 µmol m^{-2} s^{-1}. For microparticle bombardment assays and callose quantification, Arabidopsis Col-0, *cpr5-1,* and *cpr5-T3* plants were grown on ½ MS plates in the same conditions as described above for 4 weeks. Nine independent stably transformed homozygous Arabidopsis lines with single insertions for NUP62-GFP were used for fluorescence imaging (T3 segregants; 3:1 segregation) and grown on ½ MS media supplemented with 1% (w/v) sucrose and 1% (w/v) agar in a growth chamber (16 h light/8 h darkness, 23 °C, 50 µmol m^{-2} $s^{-1}$of white light, 60% humidity). For DANS assay, Arabidopsis WT and T-DNA insertion lines were grown in soil with one plant per pot at 21°C under long day conditions (16 h light/8 h dark) for 3 weeks. For analyses of the Arabidopsis shoot proteome, plants were grown in soil at 21°C under long day conditions (16 h light/8 h dark) at ~90 µmol m^{-2} sec^{-1}, 60% humidity. Respective tissues were harvested after three or five weeks. *Nicotiana benthamiana* (*N. benthamiana*) plants were grown individually in a pot under controlled conditions (16 h light/8 h darkness, 26 °C, ~90 µmol m^{-2} s^{-1}, 60% humidity).

DNA constructs

For transient expression in *N. benthamiana*, the selected NUP open reading frames (ORFs) were cloned into the binary pAB134-mVenus plasmid [6]. To generate the ORFs, total RNA was extracted from Arabidopsis leaves using the RNeasy plant mini kit (Qiagen, Hilden, Germany), and DNase I treatment was performed following the manufacturer's instructions. cDNA was then synthesized using the Maxima H Minus First Strand cDNA synthesis kit (Thermo Fisher Scientific Inc., Waltham, Massachusetts, USA). The ORFs were amplified, incorporating the Gateway attB sites, and purified PCR products were cloned into pDONR221 using a BP clonase reaction (Thermo Fisher Scientific Inc., Waltham, Massachusetts, USA). *E. coli* Stellar cells (Takara Bio) were transformed with the resulting entry vectors. Plasmids with the correct sequence were isolated and then recombined by LR reaction into the binary plant expression vector pAB134-mVenus as C-terminal mVenus fusions under the control of a β-estradiol-inducible promoter [6]. For localization of PpNUP35.1, Pp3c6_16260V3 was amplified and cloned into the binary pAB134-mVenus plasmid. For SIM experiments, XVE:CPR5-mCitrine and XVE:PDLP5-mScarlet3 were generated using GreenGate [7]. CPR5 and PDLP5 genomic sequences were amplified with primers including *Bsa*I restriction sites and ligated to pGGC000 previously digested with *Bsa*I. Resulting vectors were used to generate expression constructs using the

GreenGate modules: XVE promoter (module A), CPR5 or PDLP5 (module C), C-mCitrine or mScarlet3 (module D), HSP18.2-Terminator (module E), and the pOLE1:OLE1-RFP seed coat selection marker [8] (module F) were ligated to the linearized binary vector pGGZ003.

Monomeric enhanced GFP (mEGFP) and 2xmEGFP sequences were amplified by PCR from plasmids pENTR-R4R3-mEGFP-C (Addgene #113749) and pGGC025 (Addgene #48830), respectively, using Gateway specific primers adding the attB1 and attB2 sites and cloned into pDONR221 by BP reaction (Thermo Fisher Scientific Inc., Waltham, Massachusetts, USA). The resulting constructs, pDONR221-mEGFP and pDONR221-2xmEGFP were used for LR reaction into the destination vector pGWB502 (Addgene #74844). The p35S:3xmCherry construct was generated using GreenGate by ligating the modules Ca MV 35S promoter (Addgene #48815) (module A), 3xmCherry (Addgene #48831) (module C), HSP18.2-Terminator (module E), and the pOLE1:OLE1-RFP seed coat selection marker (module F) into the linearized binary vector pGGZ003. Topology localization of CPR5 was carried out using the split-GFP system with the vectors kindly provided by Prof. Thordal-Christensen (University of Copenhagen) [9]. pDONR-CPR5 plasmid was recombined into pDest-GW-GFP11 and pDest-GFP11-GW to generate either N- and C- fusions to the GFP 11th β-sheet using LR Gateway reactions (Thermo Fisher Scientific Inc., Waltham, Massachusetts, USA). The GFP1-10 fragment was co-expressed with either cytosolic localization (GFP1-10) or with ER-luminal localization (GFP1-10-HDEL). Plasmids pEG100-35S:nYFP-CPR5, pEG100-35S:cYFP-CPR5 and pEG100-35S:NUP93a-cYFP used for homo- and hetero-oligomerization were kindly gifted by Prof. Xinnian Dong (Duke University. North Carolina, USA) [10]. The nYFP fragment contains residues 1-172, and cYFP consists of residues 173-238. A translational fusion NUP62-GFP construct was generated from a genomic clone of *NUP62* (At2g45000), including a 1135-bp region 5'-upstream from the initiation ATG and a 407-bp region 3'-downstream from the stop codon. mEGFP was fused to the NUP62 separated by a GGGGSGGGGSGGGGS-linker [11], just before the stop codon using NEBuilder® HiFi DNA Assembly (NEB). The fluorescent protein-fusion construct was digested by *Not*I and integrated into the pBIN40 binary vector [12]. The final binary vectors were introduced into *Agrobacterium tumefaciens* strain GV3101:pMP90 and used to carry out the transformation of Arabidopsis.

We confirmed the nucleotide sequences of all constructs using standard DNA manipulation and sequencing techniques. Primers used in this study are listed in table S8.

Transient expression in *N. benthamiana* leaves

The *Agrobacterium tumefaciens* strain GV3101 (pMP90, pSOUP), containing the desired construct, was cultured overnight, then diluted to 1/10 and grown until the culture reached an OD_{600} of 0.6-0.8. Cultures were pelleted by centrifuge at 4000 rpm for 10 minutes. Bacteria were subsequently re-suspended in an Infiltration Buffer comprising 0.01 M 2-(N-morpholino) ethanesulfonic acid (MES) at pH 5.6, 0.01 M $MgCl_2$, and 150 µM acetosyringone at a final OD_{600} of 0.3. The *Agrobacterium* strain containing the intended construct was then combined with an *Agrobacterium* strain containing the P19 silencing suppressor (OD_{600} 0.1) [13]. The resulting mixture was introduced into the leaves of 4-week-old *N. benthamiana* plants through syringe infiltration. Two days after infiltration, gene expression was induced by spraying infiltrated leaves with β-estradiol solution (20 µM β-estradiol, 0.1% v/v Tween-20). Induction time was dependent on protein maturation times and ranged from 6 to 24 h. To test localization of XVE:NUP43-mCitrine at lower expression levels induction was performed with 2 µM β-estradiol and induction times did not exceed 10 h (2 µM β-estradiol, 0.1% v/v Tween-20).

For split-GFP assays, agrobacterial cultures were suspended in the Infiltration Buffer at a final OD_{600} of 0.3. *Agrobacterium* strains containing constructs split-GFP were co-infiltrated with the P19 silencing suppressor (OD_{600} 0.1) into *N. benthamiana* leaves. For split-GFP assays either GFP11-CPR5 or CPR5-GFP11 and GFP1-10 or GFP1-10-HDEL were co-infiltrated. Samples were imaged 2 days post infiltration.

Microscopy

Subcellular localization of FP fusions by confocal microcopy

Confocal microscopy was performed on a Zeiss LSM 900 (Carl Zeiss, Oberkochen, Germany) equipped with Airyscan GaAsP-PMT detectors and diode lasers using a 40x/1.20 water immersion objective (C-

Apochromat 40x/1.20 W Korr FCS). mCitrine or mVenus were excited with a 488 nm laser and emission was collected in a 520-579 nm window. GFP was excited at 488 nm and collected in a 500-550 nm window. mScarlet3 was excited at 561 nm and collected from 579-617 nm [14]. To visualize pit fields, *N. benthamiana* leaves expressing a protein of interest were infiltrated with 0.1% (w/v) aniline blue (Sigma Aldrich) solution and then imaged (excitation at 405 nm and 3-5% laser power, emission detected in a 440-480 nm window). Free mScarlet3 was expressed and excited to visualize cytoplasmic localization. Propidium iodide, a cell impermeant dye, stains the apoplasm when short incubation times are used. Thus, for visualization of the cell wall, shortly before the experiment, PI was pipetted on the object slide on the leaf disc (excitation 561 nm, 6% laser power, emission 574-617 nm). Pit fields in cotyledons of 8-day old transgenic NUP62-GFP Arabidopsis seedlings were stained by immersing leaves in 0.5% aniline blue in Sørensen's phosphate buffer [0.5% aniline blue (w/v) in 200 mM Sørensen's phosphate buffer prepared with Na_2HPO_4 and NaH_2PO_4 pH 8, Sigma-Aldrich, Saint Louis, Missouri, USA)]. For confocal imaging of NUP62-GFP Arabidopsis lines, an Eclipse Ti2 inverted microscope (Nikon) equipped with spinning disk confocal unit CSU-10 (Yokogawa) and a sCMOS camera PRIME 95B (Photometrics, Tuscon, AZ, USA) was used. GFP was excited with a 488-nm laser, and emission was collected with a 525/50-nm filter (Semrock, Rochester, New York). Images were taken with a 100x oil-immersion lens (CFI Plan Apo Lambda 1.45 NA, Nikon).

Structured Illumination Microscopy

For structured illumination microscopy (SIM), only pit fields that were not deeply embedded in the plant tissue and most proximal to the cover glass close to the objective, were observed. To do so, a *N. benthamiana* leaf disk (2-mm diameter) was immersed in water and pressed between an object slide and a high-precision coverslip (1.5H, 18 x 18 mm; A. Hartenstein) using a magnet. The sample chamber was sealed with a flexible mounting adhesive (Fixo gum; Marabu). Z-stacks with a scaling of 149-nm steps were obtained using an Elyra PS1 (Zeiss Microscopy GmbH, Oberkochen, Germany) equipped with a C-Apochromat 63x/1.2 water-immersion M27 objective. Frame size was 512 x 512 pixels. PDLP5-mScarlet3, CPR5-mCitrine, and aniline blue were excited with 561 nm, 488 nm, and 405 nm laser wavelengths, respectively. Detection filters were set for the different channels: aniline blue: bandpass (BP) 420–480/LP 750; CPR5-mCitrine: BP 495–570/LP 750; PDLP5-mScarlet3: BP 570-650/LP 655. In initial control experiments with the Elyra PS1, we observed more puncta in the green channel after excitation at 488 nm, after having used the 405 nm laser to excite aniline blue. These additional puncta in the green channel precisely overlayed with the puncta observed in the aniline blue channel. The identification of fluorescent puncta in this channel in response to excitation of aniline blue might be the result of photoconversion to longer wavelengths. To exclude possible artifacts due to photoconversion of the aniline blue, which could lead to emission in the channels used for detection of mCitrine, sequential excitation was performed at 561, 488 and 405 nm. The grating periods (grid size) for structured illumination were set to 34, 34, and 28 µm, respectively, for the three different laser wavelengths. The number of grid rotations was set to 3 rotations. Camera exposure time ranged from 49-128 ms. The setup was operated using Zeiss ZEN 2.3 SP1 software. An internal deconvolution program for SIM z-stacks was used in 3D mode with maximum isotropy, zero sectioning, and the baseline shift active for all three excitation channels. The noise filter was initially run in automatic mode, but was set to a unit below the automatic setting for the actual processing.

Callose quantification in Arabidopsis seedlings

CPR5 is involved in the activation of pattern triggered immunity (PTI) and in the repression of effector-triggered immunity (ETI) [15,16]. The *cpr5-1* mutant had previously been reported to show constitutive resistance to two virulent pathogens [17]. An important plant defense mechanism against pathogens is induction of callose deposition at PD. Elevated callose deposition in the *cpr5*-1 mutant after wounding has been reported [18]. To test whether callose deposition was increased relative to WT under the growth and experimental conditions used here, PD callose levels in WT and *cpr5-1* Arabidopsis seedlings were quantified. Leaf 5 of young seedlings (8-12 leaf stage) was stained to minimize variability. Leaves were detached with a forceps, immersed in 1% aniline blue diluted in water [1% aniline blue (w/v); Sigma-Aldrich, Saint Louis, Missouri, USA] and infiltrated by applying a vacuum in a 20 ml syringe. Aniline blue fluorescence was observed on a Zeiss LSM 900 (Zeiss Microscopy GmbH, Oberkochen, Germany) C-Apochromat 40x/1.20 W Korr FCS and GaAsP-Pmt1 detector with excitation at 405 nm, 5% laser

power and gain at 632 V. Emission was detected from 400-500 nm. Imaging parameters were consistent across all experiments. Per experiment, 3-4 leaves were assayed per genotype, 4 images were acquired per leaf. Four independent experiments were performed for WT and 5 for *cpr5-1*. Mean aniline blue fluorescence intensity was quantified with Fiji using the calloseQuant macro (calloseQuant settings: Method A, peak prominence = 55 and measurement radius = 6) [19]. Regions of Interest (ROIs) assigned to non-PD regions by the Fiji macro were removed manually. Mean aniline blue fluorescence per image was plotted.

Plasmodesmatal proteome

Preparation of *A. thaliana* plasmodesmatal (PD), cell wall (CW) and total cellular proteins (total cell extract, TC) fractions

Various Arabidopsis shoot tissues, including cauline leaves, meristem, and rosette leaves, were collected individually. Each sample pool consisted of at least six plants. PD preparation involved a minimum of three pools of the same tissue type. Tissues were freshly excised and promptly frozen in liquid nitrogen. The PD preparation protocol was based on two previously published methods [20,21]. Each pool of samples was ground in liquid nitrogen and incubated in PD extraction buffer [150 mM NaCl, 10 mM EDTA, 1 mM DTT, 1% (v/v) Triton X-100, 0.5% (v/v) sodium deoxycholate, 0.1% (w/v) SDS, 10% (v/v) glycerol, and 100 mM Tris-HCl, pH 8] with 0.5% Protease Inhibitor Cocktail (PIC, P9599, Sigma-Aldrich), 5 mM DTT, 1 mM PMSF, 50 mM NaF, 1 mM Na_3VO_4, 1 mM benzamidin and 4 µM leupeptin. For the cell wall fractions, two rounds of grinding in liquid nitrogen efficiently removed soluble protein contaminants and better prepared cell walls for digestion. The pellet was washed at least four times with a low concentration of detergents [150 mM NaCl, 10 mM EDTA, 0.1% (v/v) Triton X-100, 10% (v/v) glycerol, and 100 mM Tris–HCl, pH 8]. After the last washing step, the sample was centrifugated at 1500 x g at 4 °C with swing-out bucket (Sigma 3-30KS, Rotor 11390 & 13150). Cell wall fractions (CW; 100-200 µl) were collected from the final pellet. The rest of the CW pellet was digested in cell wall digestion buffer (1.4% cellulase, mannitol 300mM, 10 mM $CaCl_2$, 10 mM KCl) with 1 mM DTT and 0.5% PIC (P9599, Sigma-Aldrich) at room temperature for 1 h. After centrifugation, the supernatant was collected and ultracentrifuged for 80 min at 4 °C and 110,000 x g (Beckman XPN-80, Rotor SW41Ti). After ultracentrifugation, the resulting pellet was washed twice with TBS buffer (2.5 mM KCl, 140 mM NaCl and 20 mM Tris-HCl, pH 7.4 with 0.5% PIC). The final pellet was PD fraction (PD). Total protein (total cell extract, TC) was extracted according to He *et al*. [22]. All fractions were dissolved in 8M UTU (6 M urea, 2 M thiourea, Tris-HCl pH 8.0) before in-solution tryptic digestion.

Protein clean-up, trypsin digestion and peptide desalting

A single-pot, solid-phase-enhanced, sample-preparation (SP3) technology [23] with trypsin digestion was used to remove the detergent in the protein extracts. Disulfide bridges were reduced by an excess of DTT (6.5 mM), and alkylation of free cysteines was done by iodoacetamide (27 mM). SpeedBead Magnetic Carboxylate Modified Particles (SP3 beads, 45152105050250 / 65152105050250, GE Healthcare) were pre-washed by Milli-Q water. SP3 beads (50 µg/µl) were added to the protein sample in a ratio of 1:10. 50% ethanol was used for inducing protein-bead binding. After incubating 15 min at 24 °C, 1,000 rpm constant shaking, the beads were washed three times with 80% ethanol and subjected to trypsin digestion [100 mM Ammonium bicarbonate, trypsin (trypsin: protein ratio 1:100, V5113, Promega)] for 12-14 h at 37 °C. Digested proteins were acidified to pH 2 using TFA and were then desalted over C18 STAGE tips [24].

LC-MS/MS analysis of peptides

Peptide mixtures were analyzed by HPLC system nanoflow Easy-nLC (Thermo Scientific, Waltham, Massachusetts) and Orbitrap hybrid mass spectrometer (Q-exactive, Thermo Scientific). Peptides were eluted from a 75 µm x 25 cm analytical C18 column (PepMan, Thermo Scientific) on a linear gradient running from 5% to 90% acetonitrile over 70 min. Proteins were identified based on the information-dependent acquisition of fragmentation spectra of multiple charged peptides. Up to ten data-dependent MS/MS spectra were acquired in the linear ion trap for each full-scan spectrum acquired at 60,000 full-width half-maximum (FWHM) resolution.

Peptide and protein identification

MaxQuant version 2.2.0.0 was used for raw file peak extraction and protein identification against the Arabidopsis TAIR11 database (35,386 entries). The following parameters were applied: trypsin as cleaving enzyme; minimum peptide length of six amino acids; maximal two missed cleavages; carbamidomethylation of cysteine as a fixed modification; N-terminal protein acetylation, and oxidation of methionine as variable modifications. Peptide mass tolerance was set to 20 ppm, and 0.5 Da was used as the MS/MS tolerance. Multiplicity was set to 1. For label-free quantification, retention time matching between runs was chosen within a time window of two minutes. iBAQ quantification was selected within label-free quantification. The peptide false discovery rate (FDR) and the protein FDR were set to 0.01, while site FDR was set to 0.05. Hits to contaminants (e.g. keratins) and reverse hits identified by MaxQuant were excluded from further analysis. The mass spectrometry proteomics data have been deposited to the ProteomeXchange Consortium via the PRIDE partner repository [25] with the dataset identifier PXD049466.

PD score (V1.5)

The PD scoring (v1.5) was derived from the earlier PD score equation by Gombos *et al.* [1] with the modification that its components enrichment score and feature score were scaled between 0 and 1. The proteingroups.txt output from Maxquant was analyzed using Perseus. Protein iBAQ values were normalized using z-scores, and the values for PD, CW, and TC fractions were averaged across tissues (file S3). The ratios PD/CW and PD/TC were then calculated based on the average values obtained for each fraction. The PD enrichment score for each protein is the sum of PD/CW and PD/TC. The score was then scaled to a range of 0 to 1, based on the proportion of the distance to the minimum score. Regardless of the enrichment score, the feature score relies on the frequency of protein functions and PFAM domains (available at https://pfam.xfam.org/) identified within the high-confidence dataset and validated PD candidates [1,26,27]. Similar to the enrichment score, the feature score was also normalized to a scale from 0 to 1, based on the proportion of the distance to the minimum score across all *Arabidopsis* proteins (30843 entries). For each protein, the PD score (v 1.5) is obtained by summing the transformed PD enrichment score and the feature score, resulting in a range from 0 to 2. A higher PD score (1.5) indicates a greater likelihood that the protein is a PD protein.

Intercellular Transport assays

Microparticle bombardment

To test passive diffusion of 2xEGFP, microparticle bombardment was performed to deliver DNA coated gold microcarriers into single epidermal cells. 60 mg of 1.0 µm gold microcarriers (Bio-Rad Laboratories, Hercules, CA, USA) were added into a 1.5-mL microcentrifuge tube and washed with 70% ethanol before use. After the final washing step, 1 mL of 50% glycerol was added, and the tube was sealed using Parafilm® (Amcor). The suspended gold particles (35 µL) were labelled with 2 – 2.5 µg of plasmid DNA (pGWB502-p35S:2xmEGFP) in the presence of 0.1 M spermidine and 2.5 M $CaCl_2$. Tubes were vortexed for 1 min and put on ice for 1 min. Coated gold particles were centrifuged at 1,500 x g for 30 sec. The particles were washed twice with 70% ethanol. After the second washing step, 35 µL of 100% ethanol was added and vortexed until the pellet completely dispersed. This gold suspension (10 µL) was transferred onto a macrocarrier (Bio-Rad Laboratories, Hercules, CA, USA). Bombardment was performed using the PDS-1000/He Biolistic Particle Delivery System (Bio-Rad, #1652257) as described [28]. To visualize bombardments, 2xmEGFP was excited with a 488-nm laser and emission detected at 495-548 nm, while 3xmCherry was excited with a 561-nm laser and emission detected at 548-617 nm. Cells showing fluorescence in the GFP channel were counted manually on maximum projections. To identify the initially bombarded cell, Arabidopsis leaves were bombarded with gold particles coated with pGWB502-p35S:3xmCherry (84 kDa, unable to move passively through non-specific trafficking) and pGWB502-p35S:2xmEGFP. Fluorescence intensity profile plots across transects were generated using Fiji software package [29] to analyze the correlation of the fluorescence intensity of mCherry (bombarded cell) and mEGFP (fig. S9).

SHR-GFP endodermis-to-stele ratio and Fluorescence Recovery After Photobleaching (FRAP) analysis

SHR–GFP was detected in root endodermis and stele using a Zeiss LSM 900 equipped with Airyscan GaAsP-PMT detectors and diode lasers using a C-Apochromat 40x/1.20 W Korr FCS water objective. For quantification of SHR-GFP, a brief Z-stack series of up to 60 sections of short intervals (2.1 µm) around the ROI were captured, and the Sum-Projection of the volume was analyzed using ImageJ. The background fluorescence was subtracted from the average pixel intensity in the circled region in the endodermis (E) and from the average pixel intensity of the corresponding boxed region in the stele (S) (see Fig. 5D). The ratio between endodermis and corresponding stele region was calculated (E:S). Multiple samples were taken for each root to determine the average ratio.

The SHR–GFP fluorescence was bleached in endodermal cells using the 488 nm laser at full laser power for 150 iterations, which lead to around 50-70% reduction in fluorescence. 1-3 cells in the same cell layer were bleached at the same time for each root. To acquire recovery images, laser power was set to 2% to avoid bleaching. The recovery images of the bleached areas were captured every 20 min to reduce the possibility of additional bleaching from frequent scanning. To ensure the identification of the same region of interest during the time-course imaging, a brief Z-stack series of up to 60 sections with short interval (2.1µm) around the region of interest were captured. In this way, the same region should be included in the series of images and can be re-tracked later for analysis. For each time point the Sum-Projection of the same volume was analyzed. The background subtracted fluorescence intensity ratio (endodermis bleached nucleus/endodermis control nucleus) before bleach, after bleach and after 60 minutes was determined using ImageJ (see also fig. S9F for positions of ROIs). Time 0 post-bleach fluorescence was set to 0 and all measurements were normalized to this point by subtracting the time 0 post-bleach fluorescence signal from all of the pre-bleach and the recovery values. The percent recovery was calculated using the normalized values. For analysis of intracellular FRAP, a frame size of 512 × 512 pixels with a scanning speed of 0.93 ms per frame (1 Hz) and bi-directional scanning was used to accelerate the scanning rate for each frame.

DANS assay

For Drop-ANd-See (DANS) assays, 1 µl of 10 mM 5-(and 6)-carboxy-fluoresceindiacetat-acetoxymethylester (CFDA) in 0.002 % Silwet® was pipetted on the adaxial side of a rosette leaf and removed after 5 min. The 4th and 24 h later also the 5th rosette leaf was used. For microscopy, the leaf was cut off, washed in water, and mounted between two cover slips. Fluorescence was observed under an Axio Zoom.V16 (Zeiss Microscopy GmbH, Oberkochen, Germany) equipped with a X-Cite Xylts (Excelitas Technologies, PA, USA) LED light source, using a GFP broad bandpass filter cube (excitation: 470/40 nm, beam splitter: FT495 nm, emission: 525/50 nm). Images of the adaxial- and abaxial side were taken using Orca-fusionBT digital camera (C15440, Hamamatsu, Japan). Imaging parameters were consistent across experiments. To identify the fluorescent area, thresholding was performed in ImageJ with the same threshold value for adaxial-and abaxial sides. The diffusion is quantified by ratio between the area above the intensity threshold on the abaxial side and the adaxial side. Experiments of the same day were normalized to the WT experiments of the same day.

Bioinformatics

FG repeat analysis

To identify FG repeat proteins, *A. thaliana* and *P. patens* peptides encoded by gene models were downloaded from Araport 11 and Phypa_V3 genomes and screened, respectively. FG occurrences were counted in a sliding window of 200 amino acids (aa), and the maximum number of FG repeats per window was determined using a custom python script (Supplementary Script 1 and 2). Within the same script, the number of GLFG and xFxFG motifs in each peptide were counted (table S1).

PD index quantification

Overlay of fluorescence from NUP-FPs and aniline blue was quantitatively scored using the PD index [30]. To minimize bias in quantification, we employed our recently developed PD index script [1]. Briefly, clear PD sites were cropped, and channels were separated. PD were identified using auto threshold and

Fiji YEN-algorithm, with user modifications. Center coordinates of PD were determined, and square ROIs were set. The PD index was calculated by dividing mean intensity values of PD ROIs by background ROI values. Background ROIs were defined as areas of weak aniline blue fluorescence. Regions previously recognized as PD were automatically omitted from the positioning of background ROIs. Image processing was used for background ROI placement. The software Igor Pro (version 9) was used for data plotting and SPSS was used for statistical analyses.

Structure prediction for CPR5

The structure of CPR5 was predicted using Alphafold monomer version 2.3.1 [31].

Phylogenetic analyses

The tree shown in fig. S6 was generated from 68 amino acid sequences as listed in table S7. Full-length sequences were imported into the Molecular Evolutionary Genetics Analysis (MEGA) package version 11, and aligned by CLUSTALW [32]. All positions with at least 85% site coverage were used. Phylogenetic analyses were conducted using the Maximum Likelihood method. Based on the suggestions of the "find best protein model (ML)" tool in MEGA 11, the lower BIC (Bayesian Information Criterion) model was selected, which was the JTT matrix-based model [33]. A discrete Gamma distribution was used to model evolutionary rate differences among sites (five categories, +G, parameter = 6.413). Initial trees for the heuristic search were obtained automatically by applying Neighbor-Joining and BioNJ algorithms to a matrix of pairwise distances estimated using the JTT model, and then selecting the topology with a superior log likelihood value. The bootstrap consensus tree inferred from 1000 replicates was taken to represent the evolutionary history of the analyzed genes. Branches corresponding to partitions reproduced in less than 50% bootstrap replicates were collapsed.

Statistics

In the PD proteome from Arabidopsis leaf tissue, we identified 5145 proteins from PD, CW, and TC fractions, with 3347 proteins having a PD score > 0.63. Among them, 3062 proteins were quantifiable in the PD fraction, constituting our Arabidopsis shoot PD proteome. Among these, 2268 proteins were categorized as high-confidence PD proteins, while 792 proteins fall into the medium-confidence category (file S3). The PD index is based on the analysis of at least 15 images from three independent repeats for each NUP and negative control. The quantification of the intercellular spread of 2xmEGFP by counting fluorescent cells in the mEGFP channel is based on the analysis of $n_{(WT)} = 17$ independent biological experiments with in total 594 bombarded cells; $n_{(cpr5\text{-}1)} = 6$ independent biological replicates with in total 278 bombarded cells; $n_{(cpr5\text{-}T3)} = 4$ independent biological replicates with in total 99 bombarded cells. Kruskal-Wallis test with Bonferroni correction for pairwise comparison was used to test for significant differences in mean cell counts between WT, *cpr5-1*, and *cpr5-T3* with $p_{(\text{WT vs. } cpr5\text{-}1)} < 1\text{x}10^{-10}$, $p_{(\text{WT vs. } cpr5\text{-}T3)} = 0.025$, and $p_{(cpr5\text{-}1 \text{ vs. } cpr5\text{-}T3)} = 0.00005$. The *p*-values are summarized in table S2. The callose quantification is based on $n_{(WT)} = 4$ independent experiments, $n_{(cpr5\text{-}1)} = 5$ independent experiments. Student´s *t*-test indicated a non-significant difference with $p = 0.48$.

SHR-GFP endodermis-to-stele ratio is based on the quantification of $n_{(WT)} = 62$ and $n_{(cpr5\text{-}1)} = 62$ different endodermis nuclei and corresponding stele regions, while per root 3-4 different nuclei and corresponding stele regions were quantified. For endodermis-to-stele ratio, Mann-Whitney U test indicated a significant difference between WT and *cpr5-1* background with $p = 0.0006$. For baseline stele fluorescence, Mann-Whitney U test indicated no significant differences between s*hr* and s*hr x cpr5-1* with $p = 0.074$. The quantification of SHR-GFP fluorescence recovery was normalized to a control nucleus in the endodermis (see Methods and fig. S9F) and is based on n(WT) = 59 and n(*cpr5-1*) = 59 bleached nuclei, while per root 3-4 nuclei were bleached. Student´s T-Test indicated a significant difference between WT and *cpr5-1* background with p = 0.037.

For the DANS data, Kruskal-Wallis test with Bonferroni correction for pairwise comparison was used to test for significant differences between WT and mutant lines. All statistical test were performed with SPSS. In all box plots median is represented by vertical line inside the box, mean is represented by the bold +. Values between quartiles 1 and 3 are represented by box ranges, and 5th and 95th percentile are represented by error bars. Data was plotted using Igor Pro (version 9).

Supplemental Figures and Tables

table S1. Genome-wide search for potential phase-separating proteins with FG repeats. The 15 genes with the highest number of FG motifs within a 200-amino acid window in the *Physcomitrium* genome. For the list summarizing the genome-wide search for FG containing genes, see file S1. For Arabidopsis NUPs see file S2.

Gene	max #FG in 200 aa window	Predicted function
Pp3c26_7720	28	NUP96
Pp3c3_17910	28	NUP 98.1
Pp3c3_28570	25	NUP 98.2
Pp3c26_7680	25	NUP 98.3
Pp3c8_3950	21	NUP 98.4
Pp3c15_14630	19	NUP62
Pp3c14_14130	17	NUP54.1
Pp3c17_4470	16	inter-alpha-trypsin inhibitor heavy chain-related
Pp3c24_6760	14	NUP58
Pp3c13_12950	14	NUP214
Pp3c10_15930	13	NUP54.2
Pp3c10_15937	13	NUP54.3
Pp3c7_12210	12	zinc finger (CCCH-type) family protein
Pp3c24_6760	11	NUP58
Pp3c13_24530	10	Epidermal growth factor receptor substrate 15-like 1

table S2. List of known Arabidopsis NUPs and summary of localization results. *p*-values calculated from Bonferroni-corrected pairwise comparison between the tested NUP with propidium iodide marked by *; *p*-values calculated from Bonferroni-corrected pairwise comparison between the tested NUP and free mScarlet3 marked by #. Index is short for PD index (see also Fig. 2 and 3). NA: not assessed. FG-NUPs in red.

NUP	AGI	Localization at NPC	Tested for localization
NDC1	AT1G73240	membrane anchor	NA
Gp210	AT5G40480	membrane anchor	index = 1.77, * = **$2x10^{-9}$**; # = **$3x10^{-6}$**
CPR5	AT5G64930	membrane anchor	index = 1.48, * = **$7x10^{-8}$**; # = **0.0001**
PNET1	AT1G07970	membrane anchor	NA
NUP155	AT1G14850	inner ring	index = 1.34, * = **0.002**; # = 1.0
NUP93a	AT2G41620	inner ring	index = 1.38, * = **0.001**; # = 1.0
NUP35/MPPN	AT3G16310	inner ring	index = 1.36, * = **0.0002**; # = 0.549
NUP93b	AT3G57350	inner ring	index = 1.19, * = 0.43; # = 1.0
NUP188	AT4G38760	inner ring	NA
NUP205	AT5G51200	inner ring	NA
NUP160	AT1G33410	outer ring	NA
Seh1	AT1G64350	outer ring	NA
NUP96	AT1G80680	outer ring	NA
NUP133	AT2G05120	outer ring	NA
Sec13	AT2G30050	outer ring	NA
Elys/HOS1	AT2G39810	outer ring	index = 1.52, * = **$3x10^{-7}$**; # = **0.001**
NUP107	AT3G14120	outer ring	NA
NUP43	AT4G30840	outer ring	index = 1.72, * = **$3x10^{-6}$**; # = **0.006**
NUP75/85/SBB1	AT4G32910	outer ring	NA
NUP98a	AT1G10390	core FG-NUP	index = 1.38, * = **0.006**; # = 1.0
NUP54	AT1G24310	core FG-NUP	NA
NUP98b	AT1G59660	core FG-NUP	index = 1.55, * = **0.0001**; # = 0.276
NUP62	AT2G45000	core FG-NUP	index = 1.34, * = **0.0001**; # = 0.357
NUP58	AT4G37130	core FG-NUP	index = 1.37, * = **0.001**; # = 1.0
CG1	AT1G75340	cytoplasmic FG-NUP	NA
GLE1	AT1G13120	cytoplasmic NUP	NA
NUP214	AT1G55540	cytoplasmic FG-NUP	index = 1.29, * = **0.041**; # = 1.0
Rae1	AT1G80670	cytoplasmic NUP	index = 1.22, * = 0.301; # = 1.0
Aladin	AT3G56900	cytoplasmic NUP	NA
MOS7/NUP88	AT5G05680	cytoplasmic NUP	NA
NUP50a	AT1G52380	basket FG-NUP	NA
NUA/TPR/ATTPR	AT1G79280	basket	NA
NUP1/NUP136	AT3G10650	basket FG-NUP	NA
NUP50b	AT3G15970	basket FG-NUP	index = 1.06, * = 1.0; # = 1.0
NUP82	AT5G20200	basket	index = 1.24, * = 0.1; # = 1.0

table S3. PDLPs and MCTPs found in Arabidopsis shoot PD proteome. See also file S3.

PD marker	AGI
PDLP2	AT1G04520
PDLP3	AT5G43980
PDLP5	AT1G70690
MCTP3	AT3G57880
MCTP4	AT1G51570
MCTP6	AT1G22610
MCTP15	AT1G74720

table S4. NPC components identified in published cell wall/PD proteomes

NUP	Reference
CPR5	[21]
NUP93a	[27]
NUP155	[21,34,35]
SEC13	[1,21,34]
NUP205	[27]
NUA	[1]
NUP50a *	[1,21,36]
GP210	[21]
NUP35	[21]
HOS1	[21]
NUP43	[21]
NUP62	[21]
NUP214	[21]
NUP82	[21]
NDC1 *	[36]

* identified by TURBO-ID using PD proteins

table S5. Nuclear localization and observation of puncta in the cell periphery, consistent with PD localization by other laboratories

NUP	Transient expression	Stable transformation/ promoter	Reference
CPR5	*p35S:YFP-CPR5*	*p35S:GFP-CPR5/cpr5-1*	[10]
CPR5*	*p35S:CFP-CPR5*		[37]
NUP98a	*p35S:GFP-Dra2-GFP*	*p35S:NtDra2-GFP*	[38]
NUP155	*p35S:Nup155-cYFP+p35S:nYFP-CPR5*		[10]
HOS1	*p35S:HOS1-GFP*		[39]
NUP62	*p35S:Nup62-nYFP+p35S:FLC-cYFP*		[40]

* split-FP analysis indicated interaction of CPR5 with PRL1 and FIP1

table S6. Membrane/microtubule anchor proteins in NPC and ciliary gates across kingdoms

Organism/ location	# TM	Yeast	Mammalian	Chlamydomonas	Arabidopsis	*P. patens*	Ref.
NPC lumenal ring	1	POM152	GP210	n.p.	GP210	*Pp3c27_1470V3.1*	[41,42]
NPC	1	POM121	POM121	n.p.	n.p.	n.p.	
NPC	6	NDC1	NDC1	*Cre03.g197550.t1.2*	NDC1	*Pp3c23_16320V3.1*	[41,43]
NPC	3	POM33	TMEM33	*Cre02.g099650.t1.2*	*At3g02420*	*Pp3c7_9290V3.1*	this work
Ciliary gate	3	NPHP	TMEM218	*CEP290*	n.p.	n.p.	[44–48]
NPC	2	POM34	TMEM209	n.p.	PNET1 (*At1g07970*)	*Pp3c12_22070V3.1*	[48]
NPC green lineage	5	n.p.	n.p.	n.p.	CPR5	*Pp3c21_530V3.1* *Pp3c22_5670V3.1*	[10,49]

n.p. not present based on database searches

table S7. Accession numbers of CPR5 homologs used for the phylogenetic analysis shown in figure S6.

Protein name	Accession number	Species	Phylogeny	
ChabraCPR5.1	GBG69762.1	*Chara braunii*	Charophyta	Charophyceae
ChabraCPR5.2	GBG89669.1	*Chara braunii*	Charophyta	Charophyceae
ChlatCPR5	jgi|Chlat1|5100|Chrsp33S05109	*Chlorokybus atmophyticus*	Charophyta	Chlorokybophy-ceae
ClospCPR5.1	GJP55885.1	*Closterium*	Charophyta	Zygnemo-phyceae
ClospCPR5.2	GJP75531.1	*Closterium*	Charophyta	Zygnemo-phyceae
KlenitCPR5	GAQ84352.1	*Klebsormidium nitens*	Charophyta	Klebsormidio-phyceae
MesenCPR5	jgi|Mesen1|2959|ME000176S02004	*Mesotaenium endlicherianum SAG 12.97*	Charophyta	Zygnemo-phyceae
MeskraCPR5.1	jgi|Meskra657_3|1148962|CE1148961_11182	*Mesotaenium kramstae Lemmermann NIES-657 v3.0*	Charophyta	Zygnemo-phyceae
MeskraCPR5.2	jgi|Meskra657_3|1148923|CE1148922_14999	*Mesotaenium kramstae Lemmermann NIES-657 v3.0*	Charophyta	Zygnemo-phyceae
SpimuCPR5.1	jgi|Spimu1|7829|SM000018S03736	*Spirogloea muscicola CCAC 0214*	Charophyta	Spiroglo-eophycidae
SpimuCPR5.2	jgi|Spimu1|5703|SM000152S01566	*Spirogloea muscicola CCAC 0215*	Charophyta	Spiroglo-eophycidae
SpimuCPR5.3	jgi|Spimu1|9349|SM000020S05962	*Spirogloea muscicola CCAC 0216*	Charophyta	Spiroglo-eophycidae
BpraCPR5	BPRRCC1105_03G01860	*Bathycoccus prasinos*	Chlorophyta	Mamiello-phyceae
ChlodesCPR5.1	KAH7624053.1	*Chlorella desiccata (nom. nud.)*	Chlorophyta	Trebouxio-phyceae
ChlodesCPR5.2	KAG7670930.1	*Chlorella desiccata (nom. nud.)*	Chlorophyta	Trebouxio-phyceae
ChlosoroCPR5	PRW44950.1	*Chlorella sorokiniana*	Chlorophyta	Trebouxio-phyceae
ChlospCPR5	CNC64A_008G01100	*Chlorella sp NC64A*	Chlorophyta	Trebouxio-phyceae
ChlovarCPR5	XP_005848448.1	*Chlorella variabilis*	Chlorophyta	Trebouxio-phyceae
ChlovulCPR5	KAI3426217.1	*Chlorella vulgaris*	Chlorophyta	Trebouxio-phyceae
ChlpriCPR5	QDZ25445.1	*Chloropicon primus*	Chlorophyta	Chloropico-phyceae
CocsubCPR5	CV00G07110	*Coccomyxa sub-ellipsoidea C-169*	Chlorophyta	Trebouxio-phyceae
MicrocomCPR5	XP_002502434.1	*Micromonas commoda*	Chlorophyta	Mamiello-phyceae
MicropuCPR5	EuGene.0500010166|58433	*Micromonas pusilla strain CCMP1545*	Chlorophyta	Mamiello-phyceae
MicrospCPR5	M.spRCC299 v3.0|58433	*Micromonas sp or commoda RCC299 v3.0*	Chlorophyta	Mamiello-phyceae
OtCPR5	OT_02G03660	*Ostreococcus tauri*	Chlorophyta	Mamiello-phyceae
PispCPR5.1	KAI8111799.1	*Picochlorum*	Chlorophyta	Trebouxio-

		sp. BPE23		phyceae
PispCPR5.2	KAI8109780.1	*Picochlorum sp. BPE23*	Chlorophyta	Trebouxio-phyceae
MapolyCPR5.1	Mapoly0107s0002.1.p	*Marchantia polymorpha_320_v3.1*	Seedless non-tracheophyte	Marchantiopsida
MapolyCPR5.2	Mapoly0483s0001.1.p	*Marchantia polymorpha_320_v3.1*	Seedless non-tracheophyte	Marchantiopsida
MapolyCPR5.3	Mapoly0002s0001.1.p	*Marchantia polymorpha_320_v3.1*	Seedless non-tracheophyte	Marchantiopsida
PpCPR5.1	Pp3c21_530V3.1.p	*Physcomitrium patens_318_v3.3*	Seedless non-tracheophyte	Bryopsida
PpCPR5.2	Pp3c22_5670V3.1.p	*Physcomitrium patens_318_v3.3*	Seedless non-tracheophyte	Bryophyta
SphfalxCPR5	Sphfalx02G141400.1.p	*Sphagnum fallax v1.1*	Seedless non-tracheophyte	Bryophyta
DicomCPR5	Dicom.14G001200.1.p	*Diphasiastrum complanatum v3.1*	Seedless tracheophyte	Lycopodiopsida
CericCPR5	Ceric.38G046900.1.p	*Ceratopteris richardii v2.1*	Seedless tracheophyte	Polypodiopsida
AtriCPR5	ATR_00156G00170	*Amborella trichopoda*	Spermatophyta	Basal angiosperm
AtCPR5	AT5G64930	*Arabidopsis thaliana*	Spermatophyta	Dicot
BradiCPR5.1	Bradi3g57717.1.p	*Brachypodium distachyon v3.1*	Spermatophyta	Monocot
BradiCPR5.2	Bradi2g58840.1.p	*Brachypodium distachyon v3.1*	Spermatophyta	Monocot
CocitCPR5	Cocit.H3845.1.p	*Corymbia citriodora v2.1*	Spermatophyta	Dicot
GlymaCPR5	Glyma.06G145800.1.p	*Glycine max Wm82.a4.v1*	Spermatophyta	Dicot
GohirCPR5.1	Gohir.D03G045400.2.p	*Gossypium hirsutum v3.1*	Spermatophyta	Dicot
GohirCPR5.2	Gohir.A02G134000.1.p	*Gossypium hirsutum v3.1*	Spermatophyta	Dicot
HorvuCPR5.1	HORVU.MOREX.r3.6HG0618780.1	*Hordeum vulgare Morex V3*	Spermatophyta	Monocot
HorvuCPR5.2	HORVU.MOREX.r3.3HG0309890.1	*Hordeum vulgare Morex V3*	Spermatophyta	Monocot
ManesCPR5.1	Manes.13G077600.1.p	*Manihot esculenta v8.1*	Spermatophyta	Dicot
ManesCPR5.2	Manes.12G141400.1.p	*Manihot esculenta v8.1*	Spermatophyta	Dicot
NtCPR5.1	mRNA_71958	*Nicotiana tabacum K326*	Spermatophyta	Dicot
NtCPR5.2	mRNA_118909	*Nicotiana tabacum K326*	Spermatophyta	Dicot
OsCPR5.1	LOC_Os02g53070.1	*Oryza sativa_323_v7.0*	Spermatophyta	Monocot
OsCPR5.2	LOC_Os01g68970.1	*Oryza sativa_323_v7.0*	Spermatophyta	Monocot
PahalCPR5.2	Pahal.5G042600.1.p	*Panicum hallii v3.1*	Spermatophyta	Monocot
PahalCPR5.1	Pahal.1G413600.1.p	*Panicum hallii v3.2*	Spermatophyta	Monocot
PavirCPR5.1-1	Pavir.1KG111437.1.p	*Panicum virgatum v5.1*	Spermatophyta	Monocot
PavirCPR5.1-2	Pavir.1NG487400.1.p	*Panicum virgatum v5.1*	Spermatophyta	Monocot

PavirCPR5.2-1	Pavir.5NG012660.1.p	*Panicum virgatum v5.1*	Spermatophyta	Monocot
PavirCPR5.2-2	Pavir.5KG720000.1.p	*Panicum virgatum v5.1*	Spermatophyta	Monocot
PtrifCPR5	Ptrif.0007s2410.1.p	*Poncirus trifoliata v1.3.1*	Spermatophyta	Dicot
PotriCPR5.1	Potri.005G083600.1.p	*Populus trichocarpa v4.1*	Spermatophyta	Dicot
PotriCPR5.2	Potri.007G082100.1.p	*Populus trichocarpa v4.1*	Spermatophyta	Dicot
SolycoCPR5	Solyc04g054170.4.1	*Solanum lycopersicum ITAG4.0*	Spermatophyta	Dicot
StrasiaCPR5.1	GER47577.1	*Striga_asiatica_ 008636005.1_SGA_v2.0*	Spermatophyta	Dicot
StrasiaCPR5.2	GER47578.1	*Striga_asiatica 008636005.1_SGA_v2.0*	Spermatophyta	Dicot
ThuplCPR5	Thupl.29379795s0007.1.p	*Thuja plicata v3.1*	Spermatophyta	Gymnosperm
VviCPR5	VIT_207s0031g01470.1	*Vitis vinifera v2.1*	Spermatophyta	Dicot
ZmayCPR5.1	Zm00001d052145_P001	*Zea mays RefGen_V4*	Spermatophyta	Monocot
ZmayCPR5.2	Zm00001d012040_P001	*Zea mays RefGen_V4*	Spermatophyta	Monocot
ZosmaCPR5	Zosma03g20130.1	*Zostera marina v3.1*	Spermatophyta	Monocot

table S8. Primers used in this study

Primer	Sequence (5′-3′)	Description
NUP98a_Fw	TACAAAAAAGCAGGCTTCATGTTTGGCTCATCTAATCCTTTTGG	**For localization**
NUP98a_Rv	CAAGAAAGCTGGGTCAACTCCATCTTCTTCATCTTCGT	
NUP155_Fw	TACAAAAAAGCAGGCTTCAAGATGTCACAAGACGATGAG	
NUP155_Rv	CAAGAAAGCTGGGTCGAAGGAGAATGGACTTAAGAGAGACT	
NUP160_Fw	TACAAAAAAGCAGGCTTCATGGAGGAGAATCGTCGG	
NUP160_Rv	CAAGAAAGCTGGGTCACCGGTTGCAGAGGATACAG	
NUP50a_Fw	TACAAAAAAGCAGGCTTCATGGGTGACTCGGAAAACGT	
NUP50a_Rv	CAAGAAAGCTGGGTCAGTATCTGTAGCTGTTGGAGAGT	
NUP214_Fw	TACAAAAAAGCAGGCTTCAAGATGAGCAGAGTTGAGATTGAAG	
NUP214_Rv	CAAGAAAGCTGGGTCTTTTCTCATCTGTGTGAAGAGTTCC	
Rae1_Fw	TACAAAAAAGCAGGCTTCATGGCAACTTTTGGTGCGC	
Rae1_Rv	CAAGAAAGCTGGGTCTTTTCTGCCGGTTGCTCCAA	
Sec13_Fw	TACAAAAAAGCAGGCTTCAACATGCCAGGTCAGAAGATTGA	
Sec13_Rv	CAAGAAAGCTGGGTCAGGCTCAACAGCAGTAACTTGTTCC	
Elys/HOS1_Fw	TACAAAAAAGCAGGCTTCATGGATACGAGAGAAATCAACGGT	
Elys/HOS1_Rv	CAAGAAAGCTGGGTCTCTTGCTGCGAATCTACGTCT	
NUP93a_Fw	TACAAAAAAGCAGGCTTCATGGCGAACGACCAAGAGAT	
NUP93a_Rv	CAAGAAAGCTGGGTCAAAGCTTCGAGCCACCTTCTCG	
NUP62_Fw	TACAAAAAAGCAGGCTTCATGTCGGGGTTTCCATTTGGT	
NUP62_Rv	CAAGAAAGCTGGGTCAGACATCCAGTGCTTTGG	
NUP136_Fw	TACAAAAAAGCAGGCTTCCTAATGGCGAGCGCGGCAC	
NUP136_Rv	CAAGAAAGCTGGGTCTTTCTTCCTGGTGGATTTCTTTGC	
NUP107_Fw	TACAAAAAAGCAGGCTTCATGGATATGGATATGGACACTTCCC	
NUP107_Rv	CAAGAAAGCTGGGTCAGGTGATGAAAGTTCCTCTTGA	
NUP50b_Fw	TACAAAAAAGCAGGCTTCATGGGGGACTCCGATAATGC	
NUP50b_Rv	CAAGAAAGCTGGGTCCCTAGCATCTTCAGCACTCGGTGAG	
NUP35_Fw	TACAAAAAAGCAGGCTTCAAAATGAGTGCTGCAGCACACAGG	
NUP35_Rv	CAAGAAAGCTGGGTCAACACCGAACATCAAGTCAAAGA	
NUP93b_Fw	TACAAAAAAGCAGGCTTCATGGCGAACGACCAGGAG	
NUP93b_Rv	CAAGAAAGCTGGGTCAAAGCTTCGAGCTATCTTCTCG	
NUP43_Fw	TACAAAAAAGCAGGCTTCATGGAGATGATGCAGGATTCGT	
NUP43_Rv	CAAGAAAGCTGGGTCAGGCCTTGAGAAAACTGCTA	
NUP85_Fw	TACAAAAAAGCAGGCTTCAAAATGCCGGGTATGTCTTCGGA	
NUP85_Rv	CAAGAAAGCTGGGTCACATTCTTCGAGAAAAGCACGT	
NUP58_Fw	TACAAAAAAGCAGGCTTCATGTCGTTTTTTCCCCCAC	
NUP58_Rv	CAAGAAAGCTGGGTCTGTACGGCGTGTAGTTCGAGATTTT	
NUP82_Fw	TACAAAAAAGCAGGCTTCGAGTTCATGGCCACTCAAGGAGAAGC	
NUP82_Rv	CAAGAAAGCTGGGTCTGTCTTACAGCAGACACCGTCACTT	
Gp210_Fw	TACAAAAAAGCAGGCTTCATGGTTCCCGTCTCGTTCTG	
Gp210_Rv	CAAGAAAGCTGGGTCCATAGTGTTTTGAGGATTAAACC	
NUP205_Fw	TACAAAAAAGCAGGCTTCATGGTGTCGCCGAAAGATTT	
NUP205_Rv	CAAGAAAGCTGGGTCTACACACTTTTGGATGGCCA	
CPR5_Fw	TACAAAAAAGCAGGCTTCTTTAAGGCTATGGAAGCCCTCCTCC	
CPR5_Rv	CAAGAAAGCTGGGTCCTCGTCAGCATAGTCAGACCCACCA	
GGBmScarlet3F	AAAGGTCTCAAACAATGGACAGTACCGAAGCT	
GGBmScarlet3R	AAAGGTCTCAAGCCGGATCCCCCGGAGC	
PpNUP98.1_Fw	TGTACAAAAAAGCAGGCTTAATGTTTGGATCCAGCAGCCC	
PpNUP98.1_Rv	TGTACAAGAAAGCTGGGTAATCAAAATCCAGACCATATCCACTG	
PpNup62_Fw	TGTACAAAAAAGCAGGCTTAATGTCGGGCTTCACAGGATT	
PpNup62_Rv	TGTACAAGAAAGCTGGGTAGGCTCCACGCAAACGAGATC	
PpNup58_Fw	TGTACAAAAAAGCAGGCTTAATGGCGGGGATGTTCCAAAC	
PpNup58_Rv	TGTACAAGAAAGCTGGGTACTTTCGACGTGTGCCAC	

PpNup35.1_Fw	TACAAAAAAGCAGGCTTCATGAGTACCCCAGGCGCG	
PpNup35.1_Rv	CAAGAAAGCTGGGTCCATACCAAATACAAAATCCACAAATT	
PDLP5_SIM_Fw	TTTGGTCTCAGGCTCTATGATCAAGACAAAGACGACG	**For SIM**
PDLP5_SIM_Rv	TTTGGTCTCACTGATTTACACCATTTCTCATCTGCA	
CPR5_SIM_Fw	TTTGGTCTCAGGCTCTATGGAAGCCCTCCTCCTC	
CPR5_SIM_Fw	TTTGGTCTCACTGAAGCATAGTCAGACCCACC	
GGDmScarlet3F	AAAGGTCTCATCAGGTATGGACAGTACCGAAGCT	
GGDmScarlet3R	AAAGGTCTCAGCAGGGATCCCCCGGAGC	
CPR5_Topol_Rv	GGGGACCACTTTGTACAAGAAAGCTGGGTATCAAGCATAGTCAGACCCACC	**For CPR5 topology**
mEGFP_Fw	GGGGACAAGTTTGTACAAAAAAGCAGGCTTCACCATGGTGAGCAAGGGCGAGG	**For microparticle bombardment**
mEGFP_Rv	GGGGACCACTTTGTACAAGAAAGCTGGGTGTTACTTGTACAGCTCGTCCATGCC	
2xmEGFP_Fw	GGGGACAAGTTTGTACAAAAAAGCAGGCTTCACCATGGTTTCTAAGGGTGAGG	
2xmEGFP_Rv	GGGGACCACTTTGTACAAGAAAGCTGGGTGTTACTTGTACAGCTCGTCCATGCC	
NUP62_F	GCTTTTTCTATTGAGGTTCAAACTTGTAAGC	**For transgenic line expressing NUP62-GFP**
NUP62_R	CCGGTCAAGAGAAATATAATAATCTCTG	
NUP62_U1	AGACATCCAGTGCTTTGGAGCC	
NUP62_D1	TGATAAGAATTACAAAAACCACATAATCTC	
NUP62GFP_HiFiF	AAGCACTGGATGTCTGGTGGAGGCGGTTCAGGCGGAGGTGG	
NUP62GFP_HiFiR	TTGTAATTCTTATCACTTGTACAGCTCGTCCATGCCGTG	

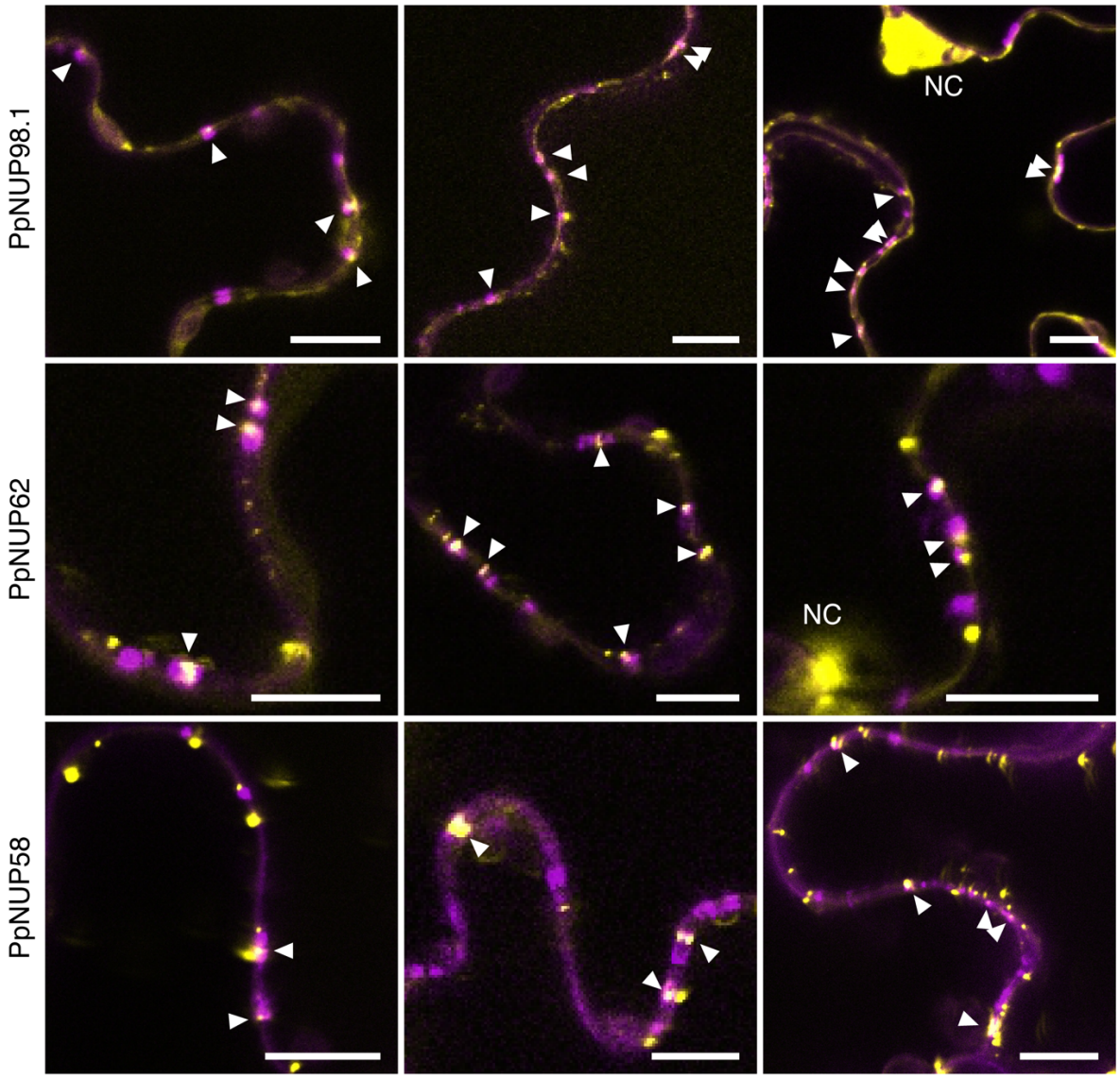

figure S1. Overlay of *Physcomitrium patens* FG-NUPs with the PD marker aniline blue. Localization of FG-NUPs from *P. patens* in *N. benthamiana* epidermal cells visualized by confocal microscopy. FG-NUPs were fused at their C-terminus to mVenus (yellow) and expressed transiently under the control of the inducible XVE promotor. Aniline blue (purple) was infiltrated to stain callose, which accumulates in pit fields. Arrowheads indicate overlay between NUPs and aniline blue. For each NUP, a similar localization pattern appeared in at least three independent experiments. NC = nucleus. Scale bar: 10 µm.

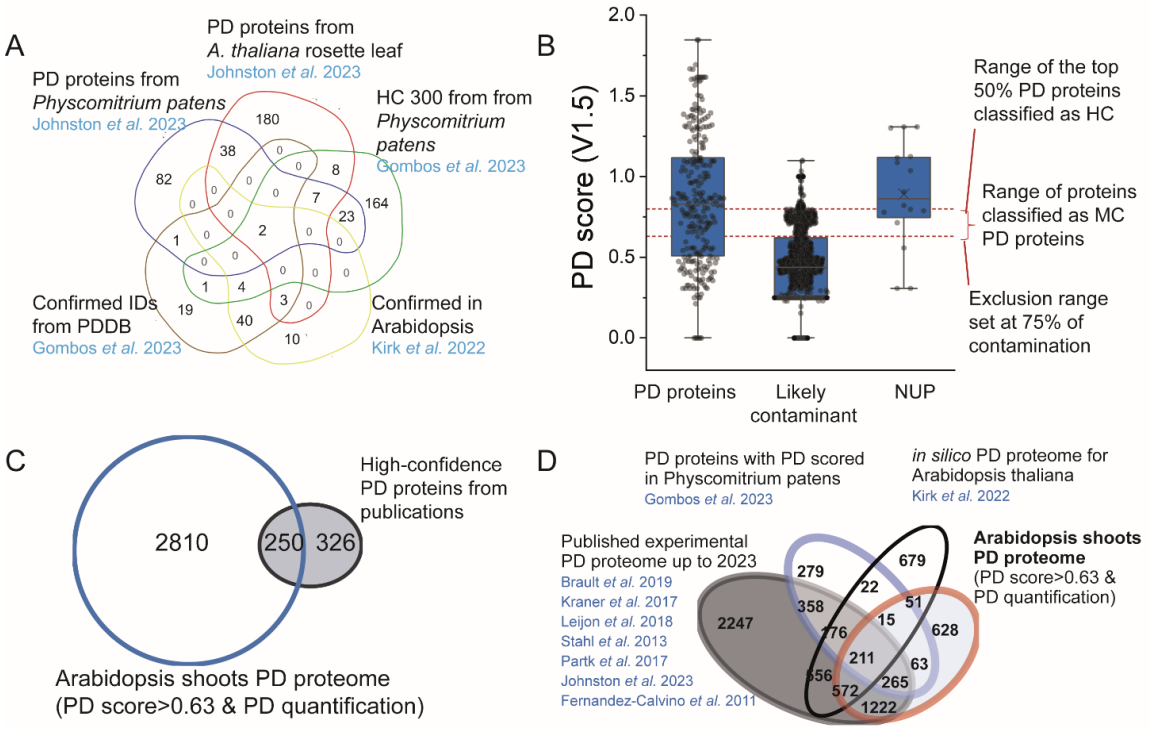

figure S2. Arabidopsis shoot proteome and the comparison to other PD proteomes. (**A**), Venn diagram defining high-confidence PD proteins from previous publications, e.g., confirmed Arabidopsis PD proteins from studies by Kirk *et al.* (2022) and Gombos *et al.* (2023), and high confidence PD proteins identified in *Physcomitrium* from studies by Gombos *et al.* (2023), and in both *Physcomitrium* and Arabidopsis leaves by Johnston *et al.* (2023) (*1*, *26*, *27*). These proteins were then used as high-confidence data set to establish the PD probability threshold and were labelled as 'PD proteins' in file S3. 43% of these proteins were quantified in our Arabidopsis shoot PD proteome. (**B**), PD Scores of nuclear pore components. PD Scores (v 1.5) are shown as box plots for high-confidence PD proteins (PD proteins), typical co-purifying proteins from plastid and mitochondria identified in Arabidopsis PD preparations (likely contaminants) and proteins of the nuclear pore complex (NUP). Dotted lines indicate two thresholds based on the frequency distribution for contaminant proteins and PD proteins. The median is shown as a gray line, the mean value is denoted by a + symbol, and the whiskers cover the 95thpercentile. PD Scores above 0.83 (the upper dotted line) indicate high-confidence (HC) PD proteins; scores between 0.63 and 0.83 (between the two dotted lines) signify medium-confidence (MC) PD proteins; and scores below 0.63 are considered low confidence (LC) as their PD Scores overlapped with 75% of the contaminants. These confidence clusters were annotated in file S3. The final Arabidopsis shoot PD proteome consists of proteins with PD scores above 0.63, which are also quantifiable in the PD fraction. (**C**), Overlap between the Arabidopsis shoot PD proteome and other PD proteomes. Proteins with a PD score >0.63 and quantifiable in PD fraction (Arabidopsis shoot PD proteome) were compared with nine representative PD proteome studies. In the current Arabidopsis shoot PD proteome, 80% of the proteins were previously identified in published PD proteomes. Combining PD enrichment and data analysis thresholding allowed us to determine the confidence levels of PD proteins and obtain a "cleaner" PD proteome. In total, we identified 5145 proteins from PD, CW, and TC fractions, with 3347 proteins having a PD score >0.63. Among them, 3062 proteins are quantifiable in the PD fraction, constituting our Arabidopsis shoot PD proteome. Among these, 2268 proteins are categorized as high-confidence PD proteins, while 792 proteins fall into the medium-confidence category (file S3). Additionally, we discovered 20 nuclear pore proteins (NUPs), with 15 of them surpassing the threshold and being included in the final PD proteome. Among these, 11 are classified as high-confidence PD proteins, while 4 are medium-confidence PD proteins (file S3, fig. S2B). (**D**) Comparison of Arabidopsis shoot PD proteomes with various published PD proteomes. 80% of the proteins had been identified in previous studies.

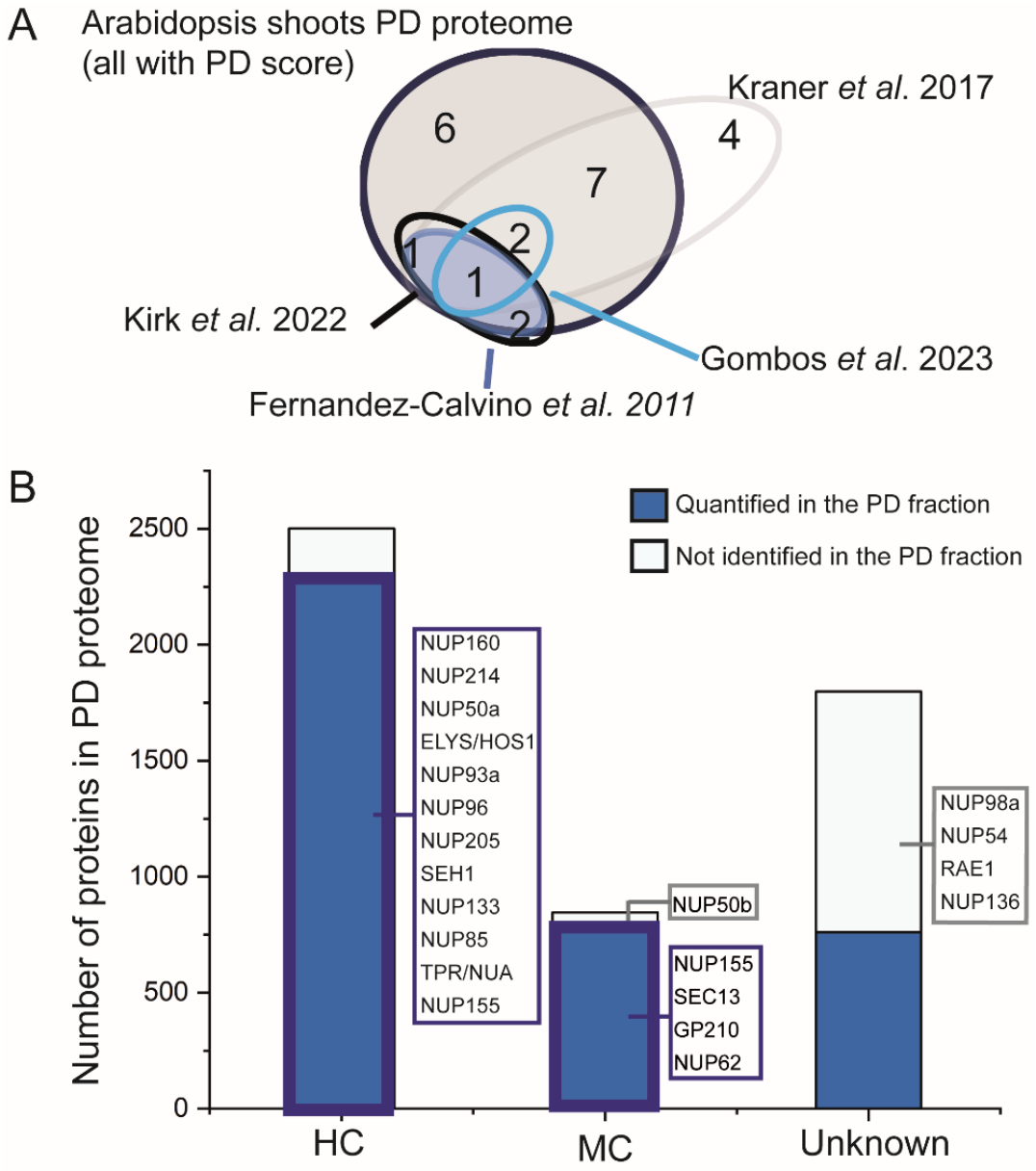

figure S3. NUPs are found in Arabidopsis shoot proteome and other PD proteomes. (A), Comparison of NUPs in Arabidopsis shoot PD proteomes with published PD proteomes. Among the NUPs identified in the Arabidopsis shoot PD proteome, 73.3% (11 out of 15) were also detected in previously published PD proteomes. (**B**), Overview of identified proteins in the PD proteome. HC (PD score > 0.83), MC (0.83 > PD score > 0.63), and Unknown (PD score < 0.63). Purple-edged boxes in HC and MC mark proteins that meet Arabidopsis shoot PD proteome criteria (PD score > 0.63, quantifiable in PD fraction). Blue bars denote 16 NUPs within the Arabidopsis shoot PD proteome; white bars represent NUPs found also in other proteomes.

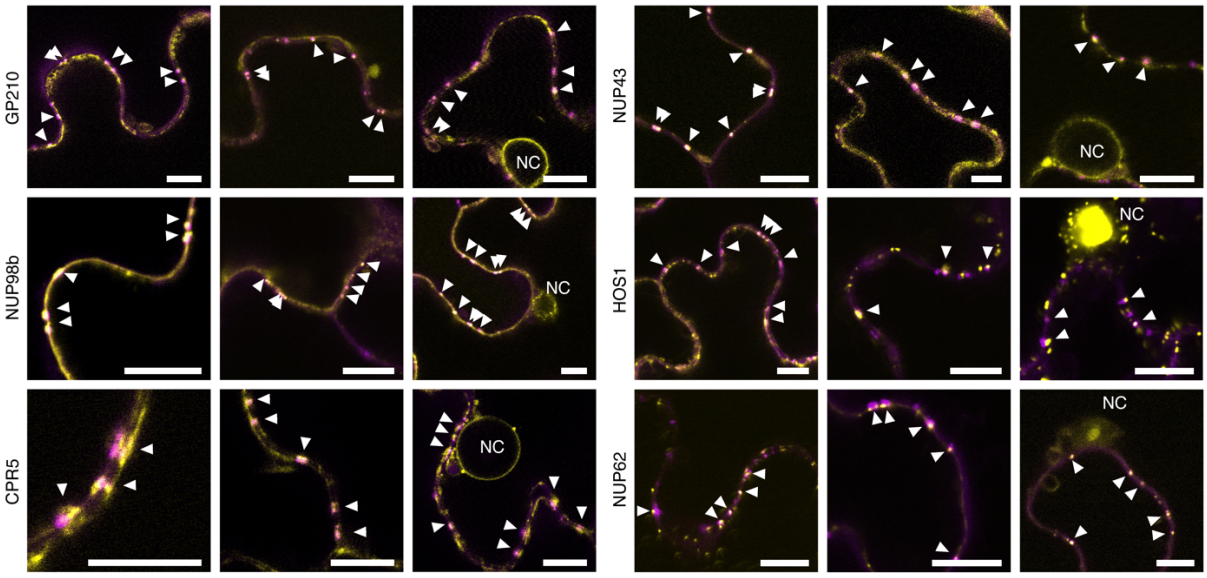

figure S4. Arabidopsis NUP-FP localization overlays with a PD marker. Localization of Arabidopsis NUPs in *N. benthamiana* epidermal cells visualized by confocal microscopy. NUPs were fused at their C-terminus to mVenus or mCitrine (yellow) and expressed transiently under the control of the inducible XVE promotor. Aniline blue (purple) was infiltrated to stain callose that accumulates in pit fields. Arrowheads indicate overlay between NUPs and aniline blue. NUPs shown here were found to have a significant increased PD index values compared to negative controls in Fig. 2. For each NUP, the localization pattern was reproducible in at least in three independent experiments. NC, nuclei. Note that for comparison, we here show the same images for NUP98B and NUP62 from Fig. 2A again. Scale bar: 10 µm.

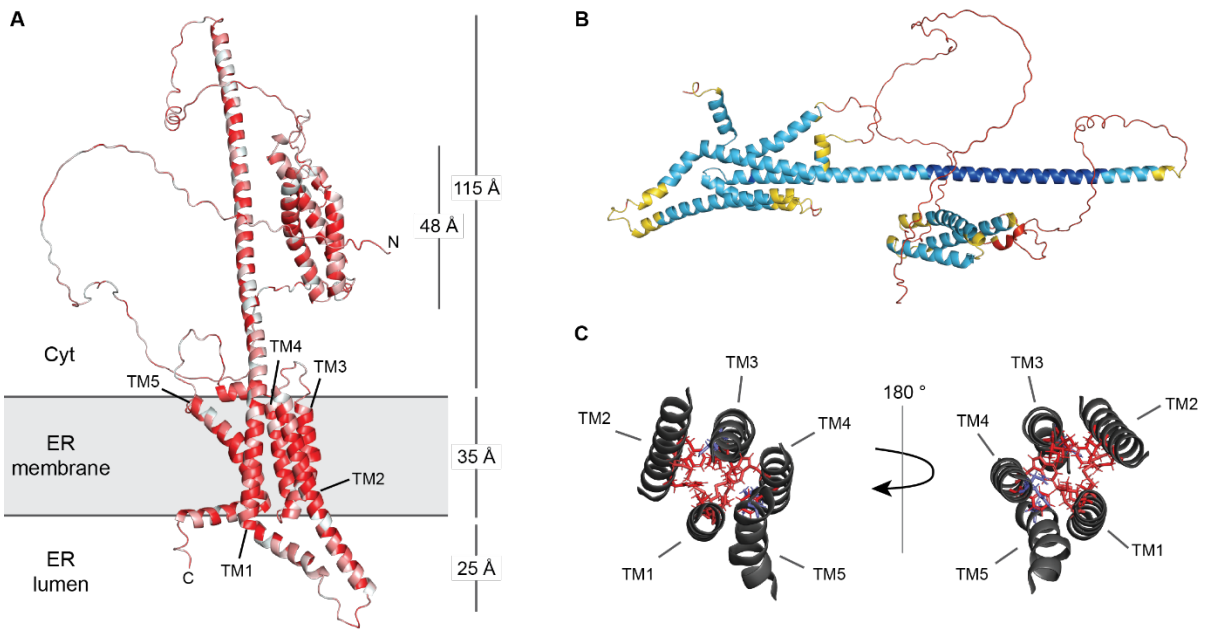

fig. S5. Predicted structure of monomeric CPR5 and model for integration into ER-derived membranes. Topological studies using the split-GFP system (Fig. 4A,B, fig. S7) are consistent with a localization of the CPR5 C-terminus in the ER lumen, while its N-terminus extends into the cytoplasm. (**A**), CPR5 is composed of a N-terminal, disordered region (residues 1-106), a soluble domain formed by 3 α-helices (107-192), linked by a second disordered region (193- 265) to an approx. 115 Å long, central α-helix (266-342). Hydrophobic residues (red) of the central helix (TM1) and 4 shorter helices (TM2-TM5) form a transmembrane domain spanning approx. 35 Å, consistent with the expected thickness for ER-derived membranes. C-terminus and helical extensions of TM1 and TM2 reach into the ER lumen. (**B**), Structure colored by per-residue prediction confidence (pLDDT; dark blue: 90-100, light blue: 50-70, yellow: 50-70, red: < 50). Low confidence values (red) may indicate regions that are either intrinsically disordered or assume a structure when interacting with other proteins and therefore could partake in formation of complexes with NUPs. (**C**), View of transmembrane helical bundle from ER lumen (left) and cytoplasm (right). Amino acid side chains spanning between transmembrane helices are colored by hydrophobicity (blue: hydrophilic, red: hydrophobic). The CPR5 transmembrane domain is not predicted to form a solvent-accessible pore.

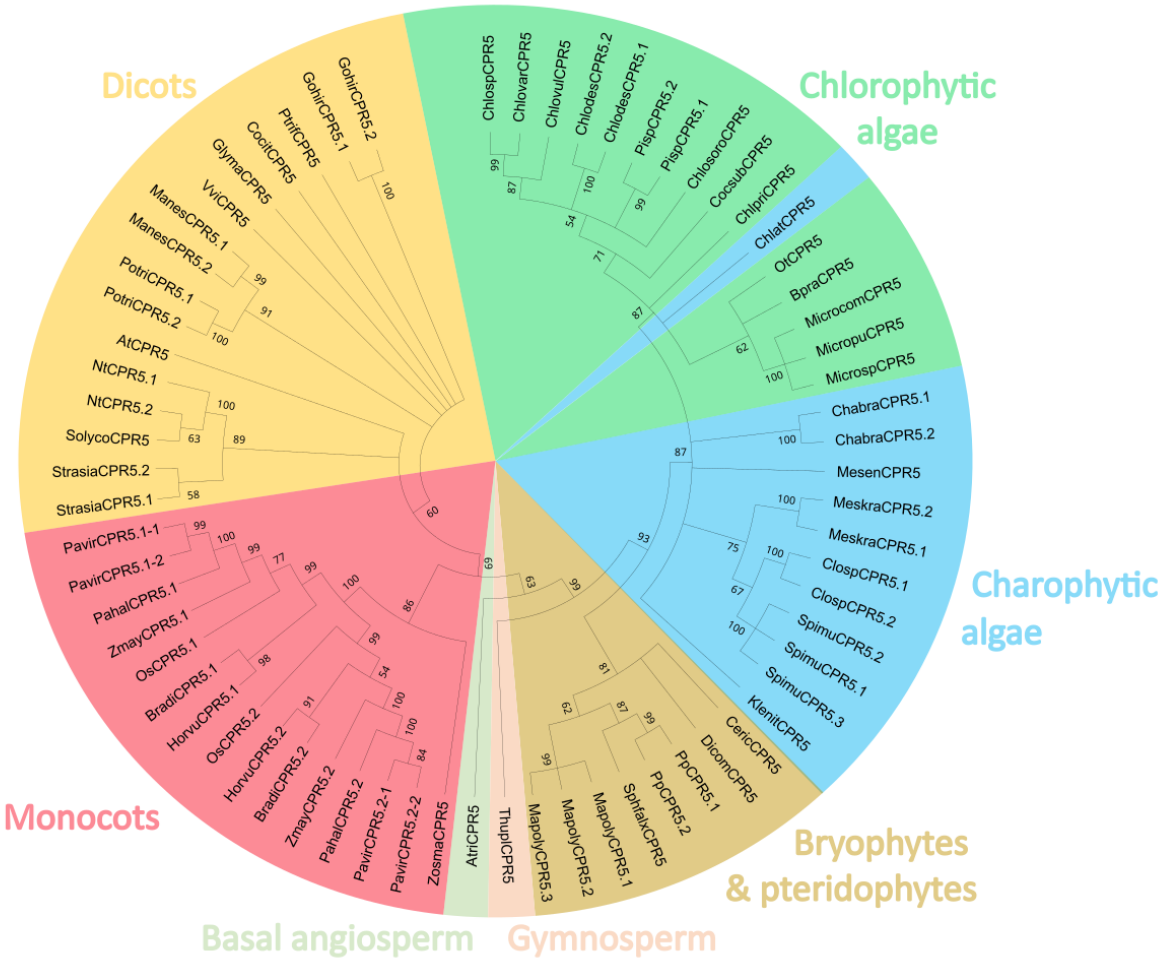

figure S6: Phylogenetic analysis of CPR5 sequences. The accession numbers and the abbreviations corresponding to the mature protein sequences used for this analysis are given in table S7. The analysis was performed as described in the “Materials and Methods” section.

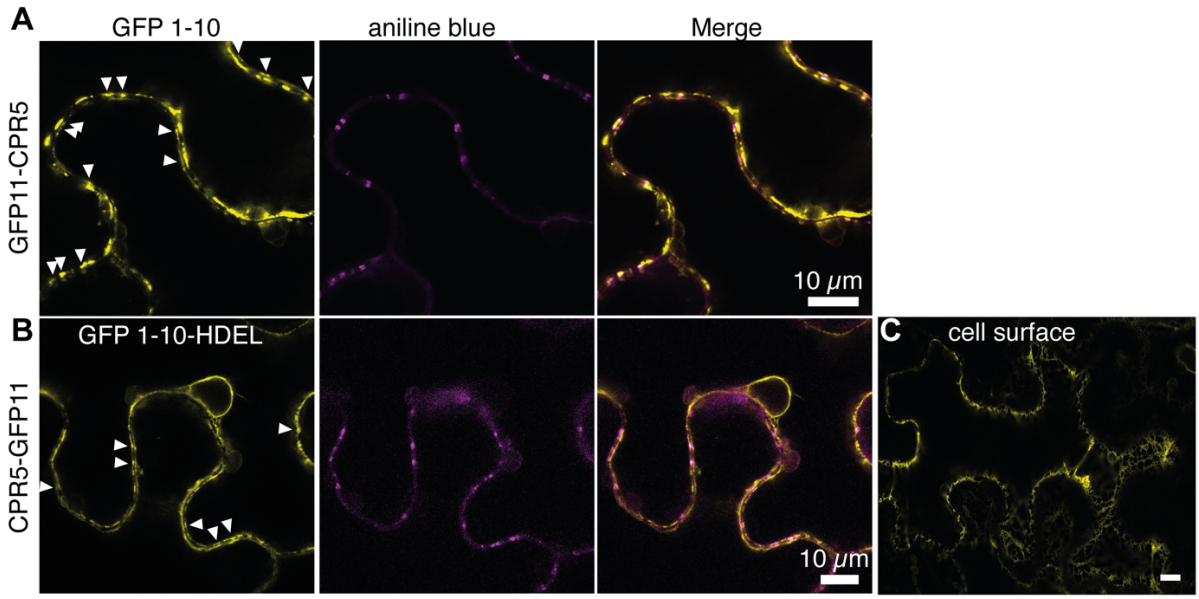

figure S7. The C-terminus of CPR5 faces ER lumen. (A), Transient co-expression of GFP11-CPR5 and cytosolic GFP1-10 in *N. benthamiana* leaves, same cell as shown in Fig. 4. *Left*, GFP channel. Reconstitution can be observed also at PD (arrowheads). *Middle*, aniline blue. *Right,* merge. **(B),** *N. benthamiana* epidermal cells transiently expressing CPR5-GFP11 and ER luminal GFP1-10-HDEL, same cell as shown in Fig. 4. *Left*, GFP channel. Reconstitution can be observed also at PD (arrowheads); *middle*, aniline blue*; right,* merge. **(C)**, Surface view of the same cell as in B, showing reconstitution in the ER.

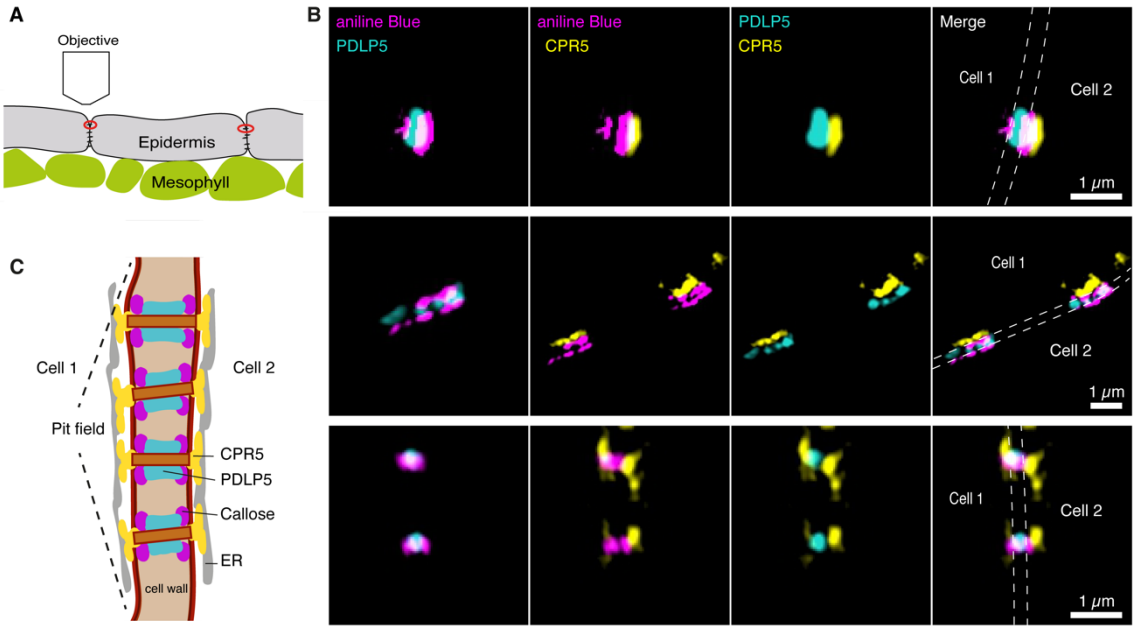

figure S8. **CPR5-mCitrine localizes at the orifices of PD**. **(A),** Cartoon showing analyzed PD: only PD most proximal to the cover glass and objective were analyzed to reduce effects caused by scattering of light due to cell wall. **(B),** SIM in *N. benthamiana* leaves co-infiltrated with XVE:PDLP5-mScarlet3 and XVE:CPR5-mCitrine. Prior to the imaging, leaves were infiltrated with aniline blue. PDLP5-mScarlet3 in turquoise, CPR5-mCitrine in yellow, and aniline blue in magenta. Comparable results were obtained in four independent experiments. Dashed lines indicate approximation of cell wall boundaries. **(C),** Cartoon of pit field and localization of PDLP5 and CPR5. Fluorescence reporting on CPR5 in (B) extends laterally 200-1000 nm in the epidermal cell wall. Previously, the lateral extension of individual PD pores in the cell wall was estimated to 100 nm for basal trichome cell walls and 187 nm for epidermal cell walls [50,51]. The resolution achieved with SIM was not high enough to resolve single PD or determine whether pit fields consist of several simple PD (as shown in C) or a few complex (H-shaped/twinned) PD.

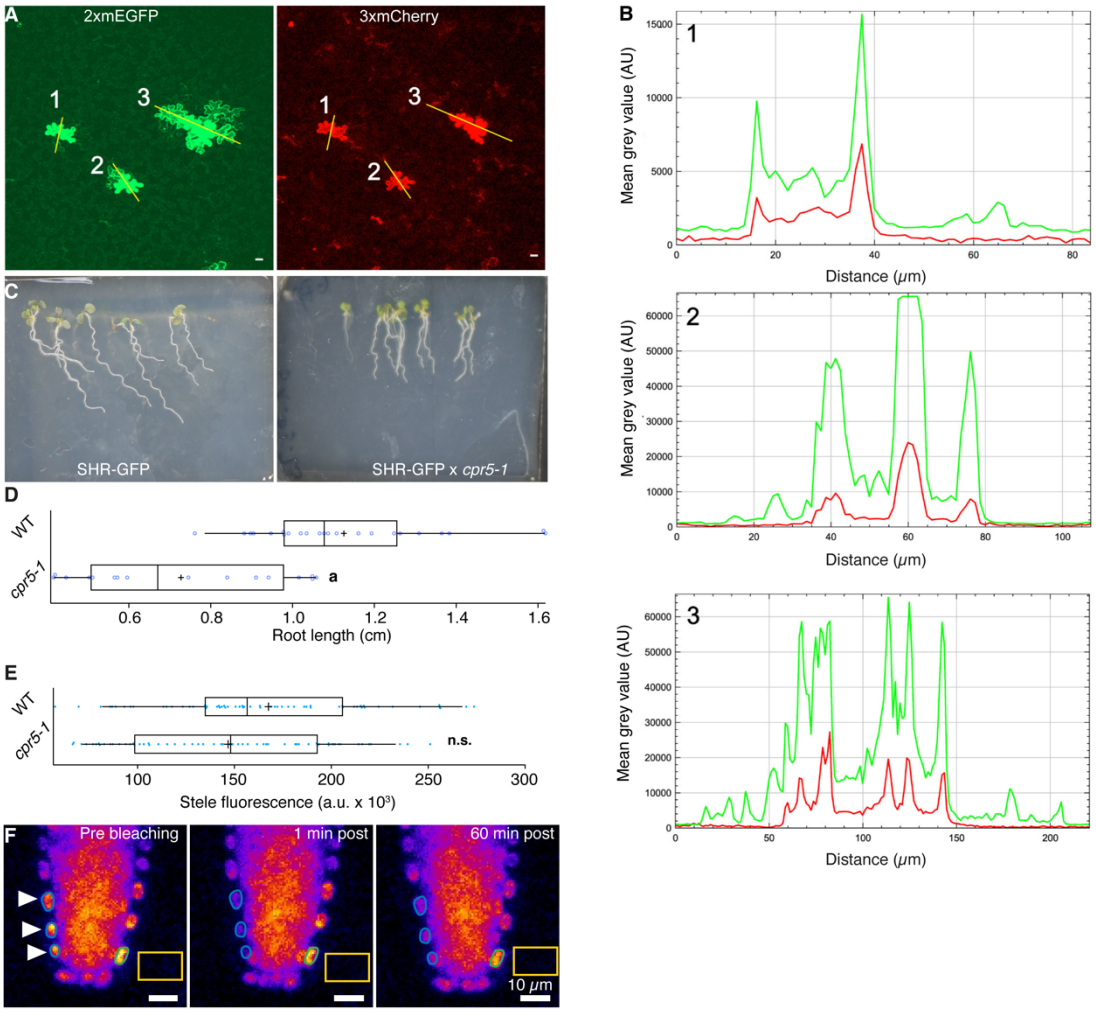

figure S9. Intercellular transport assays in *cpr5-1* mutants. (A), Example of three different clusters (1, 2, and 3) of fluorescent cells after bombardment in a WT Arabidopsis leaf. Each cluster reports a successful bombardment event. Left, GFP channel, right, mCherry channel. 24 h prior to the experiment, leaves were co-bombarded with gold particles coated with p35S:mEGFP-mEGFP (2xmEGFP). DNA plasmids and gold particles coated with p35S:mCherry-mCherry-mCherry (3xmCherry). **(B),** Profile plots across the different clusters, 1, 2, and 3 as shown in A. Yellow lines in A indicate the position for the profile. The bombarded cell marked with 3xmCherry overlays with the brightest cell in the GFP channel. **(C),** Six-day old seedlings with *shr*/pSHR:SHR-GFP in WT Col-0 background *(left)* and *shr*/pSHR:SHR-GFP in the *cpr5-1* background (*right*) grown on ½ MS agar. **(D),** Quantification of the root length of 6-day old WT and *cpr5-1* mutant background seedlings. $n_{(WT)} = 23$ roots, four independent experiments, $n_{(cpr5\text{-}1)} = 16$ roots, three independent experiments. **a** Significantly decreased root length in *cpr5-1* mutant, based on Student´s *t*-test with $p = 0.00002$. **(E),** Quantification of SHR-GFP stele baseline fluorescence in *cpr5-1* mutant and WT background. $n_{(WT)} = 62$ stele ROIs, $n_{(cpr5\text{-}1)} = 62$ stele ROIs, with 3-4 ROIs analyzed per root. **n.s.,** no significant difference in fluorescence intensity based on Mann-Whitney U test with $p = 0.074$. **(F)**, SHR–GFP fluorescence recovery after photobleaching (FRAP) in homozygous *shr*/pSHR:SHR-GFP root endodermal cells (arrow heads). Note that for comparison, we here show the same sum projections as in Fig. 5F (*top*). Blue circles show the position of ROIs for FRAP. Green circle shows the position of ROI for control nucleus used for normalization (see Methods). Yellow square shows the position for mean background fluorescence used for correction (see Methods).

References

1. Gombos, S. *et al.* A high-confidence *Physcomitrium patens* plasmodesmata proteome by iterative scoring and validation reveals diversification of cell wall proteins during evolution. *New Phytol.* **238**, 637–653 (2023).
2. Bowling, S. A. *et al.* A mutation in Arabidopsis that leads to constitutive expression of systemic acquired resistance. *Plant Cell* **6**, 1845–5187 (1994).
3. Wang, F. *et al.* Arabidopsis CPR5 regulates ethylene signaling via molecular association with the ETR1 receptor. *J. Integr. Plant Biol.* **59**, 810–824 (2017).
4. Cui, H. *et al.* An evolutionarily conserved mechanism delimiting SHR movement defines a single layer of endodermis in plants. *Science* **316**, 421–5 (2007).
5. Dyachok, J., Yoo, C.-M., Palanichelvam, K. & Blancaflor, E. B. Sample preparation for fluorescence imaging of the cytoskeleton in fixed and living plant roots. in *Cytoskeleton Methods and Protocols* (ed. Gavin, R. H.) 157–169 (Humana Press, Totowa, NJ, 2010). doi:10.1007/978-1-60761-376-3_8.
6. Bleckmann, A., Weidtkamp-Peters, S., Seidel, C. A. & Simon, R. Stem cell signaling in Arabidopsis requires CRN to localize CLV2 to the plasma membrane. *Plant Physiol.* **152**, 166–76 (2010).
7. Lampropoulos, A. *et al.* GreenGate - a novel, versatile, and efficient cloning system for plant transgenesis. *PLOS ONE* **8**, e83043 (2013).
8. Shimada, T. L., Shimada, T. & Hara-Nishimura, I. A rapid and non-destructive screenable marker, FAST, for identifying transformed seeds of *Arabidopsis thaliana*. *Plant J.* **61**, 519–528 (2010).
9. Xie, W., Nielsen, M. E., Pedersen, C. & Thordal-Christensen, H. A Split-GFP gateway cloning system for topology analyses of membrane proteins in plants. *PLOS ONE* **12**, e0170118 (2017).
10. Gu, Y. *et al.* Nuclear pore permeabilization is a convergent signaling event in effector-triggered immunity. *Cell* **166**, 1526-1538.e11 (2016).
11. Shimozono, S. & Miyawaki, A. Engineering FRET constructs using CFP and YFP. in *Methods in Cell Biology* vol. 85 381–393 (Academic Press, 2008).
12. Miyashima, S., Koi, S., Hashimoto, T. & Nakajima, K. Non-cell-autonomous microRNA165 acts in a dose-dependent manner to regulate multiple differentiation status in the Arabidopsis root. *Development* **138**, 2303–2313 (2011).
13. Qu, F. & Morris, T. J. Efficient infection of *Nicotiana benthamiana* by tomato bushy stunt virus Is facilitated by the coat protein and maintained by p19 through suppression of gene silencing. *Mol. Plant-Microbe Interactions®* **15**, 193–202 (2002).
14. Gadella, T. W. J. *et al.* mScarlet3: a brilliant and fast-maturing red fluorescent protein. *Nat. Methods* **20**, 541–545 (2023).
15. Ma, M. *et al.* CPR5 positively regulates pattern-triggered immunity via a mediator protein. *J. Integr. Plant Biol.* **65**, 1613–1619 (2023).
16. Wang, S. *et al.* A noncanonical role for the CKI-RB-E2F cell-cycle signaling pathway in plant effector-triggered immunity. *Cell Host Microbe* **16**, 787–794 (2014).
17. Bowling, S. A., Clarke, J. D., Liu, Y., Klessig, D. F. & Dong, X. The cpr5 mutant of Arabidopsis expresses both NPR1-dependent and NPR1-independent resistance. *Plant Cell* **9**, 1573–84 (1997).
18. Kohler, A., Schwindling, S. & Conrath, U. Benzothiadiazole-induced priming for potentiated responses to pathogen infection, wounding, and infiltration of water into leaves requires the *NPR1/NIM1* gene in Arabidopsis. *Plant Physiol.* **128**, 1046–1056 (2002).
19. Huang, C., Mutterer, J. & Heinlein, M. In vivo aniline blue staining and semiautomated quantification of callose deposition at plasmodesmata. in *Plasmodesmata: Methods and Protocols*

(eds. Benitez-Alfonso, Y. & Heinlein, M.) 151–165 (Springer US, New York, NY, 2022). doi:10.1007/978-1-0716-2132-5_9.

20. Faulkner, C. & Bayer, E. M. Isolation of plasmodesmata. *Methods Mol. Biol.* **1511**, 187–198 (2017).
21. Kraner, M. E., Müller, C. & Sonnewald, U. Comparative proteomic profiling of the choline transporter-like1 (CHER1) mutant provides insights into plasmodesmata composition of fully developed *Arabidopsis thaliana* leaves. *Plant J. Cell Mol. Biol.* **92**, 696–709 (2017).
22. He, M., Wang, J., Herold, S., Xi, L. & Schulze, W. X. A rapid and universal workflow for label-free-quantitation-based proteomic and phosphoproteomic studies in cereals. *Curr. Protoc.* **2**, e425 (2022).
23. Hughes, C. S. *et al.* Single-pot, solid-phase-enhanced sample preparation for proteomics experiments. *Nat. Protoc.* **14**, 68–85 (2019).
24. Rappsilber, J., Ishihama, Y. & Mann, M. Stop and go extraction tips for matrix-assisted laser desorption/ionization, nanoelectrospray, and LC/MS sample pretreatment in proteomics. *Anal. Chem.* **75**, 663–670 (2003).
25. Deutsch, E. W. *et al.* The ProteomeXchange consortium in 2020: enabling 'big data' approaches in proteomics. *Nucleic Acids Res.* **48**, D1145–D1152 (2020).
26. Johnston, M. G. *et al.* Comparative phyloproteomics identifies conserved plasmodesmal proteins. *J. Exp. Bot.* **74**, 1821–1835 (2023).
27. Kirk, P., Amsbury, S., German, L., Gaudioso-Pedraza, R. & Benitez-Alfonso, Y. A comparative meta-proteomic pipeline for the identification of plasmodesmata proteins and regulatory conditions in diverse plant species. *BMC Biol.* **20**, 128 (2022).
28. Tee, E. E., Samwald, S. & Faulkner, C. Quantification of cell-to-cell connectivity using particle bombardment. *Methods Mol. Biol. Clifton NJ* **2457**, 263–272 (2022).
29. Schindelin, J. *et al.* Fiji: an open-source platform for biological-image analysis. *Nat. Methods* **9**, 676–82 (2012).
30. Grison, M. S. *et al.* Plasma membrane-associated receptor-like kinases relocalize to plasmodesmata in response to osmotic stress. *Plant Physiol.* **181**, 142–160 (2019).
31. Jumper, J. *et al.* Highly accurate protein structure prediction with AlphaFold. *Nature* **596**, 583–589 (2021).
32. Tamura, K., Stecher, G. & Kumar, S. MEGA11: Molecular Evolutionary Genetics Analysis Version 11. *Mol. Biol. Evol.* **38**, 3022–3027 (2021).
33. Jones, D. T., Taylor, W. R. & Thornton, J. M. The rapid generation of mutation data matrices from protein sequences. *Bioinformatics* **8**, 275–282 (1992).
34. Bayer, E. M. *et al.* Arabidopsis cell wall proteome defined using multidimensional protein identification technology. *PROTEOMICS* **6**, 301–311 (2006).
35. Fernandez-Calvino, L. *et al.* Arabidopsis plasmodesmal proteome. *PloS One* **6**, e18880 (2011).
36. Li, Z., Liu, S.-L., Montes-Serey, C., Walley, J. W. & Aung, K. PLASMODESMATA-LOCATED PROTEIN 6 regulates plasmodesmal function in Arabidopsis vasculature. *Plant Cell* **36**, 3543–3561 (2024).
37. Peng, S. *et al.* CONSTITUTIVE EXPRESSER OF PATHOGENESIS-RELATED GENES 5 is an RNA-binding protein controlling plant immunity via an RNA processing complex. *Plant Cell* **34**, 1724–1744 (2022).
38. Gallemí, M. *et al.* DRACULA2 is a dynamic nucleoporin with a role in regulating the shade avoidance syndrome in Arabidopsis. *Development* **143**, 1623–1631 (2016).

39. Lee, J. H. *et al.* The E3 ubiquitin ligase HOS1 regulates low ambient temperature-responsive flowering in *Arabidopsis thaliana*. *Plant Cell Physiol.* **53**, 1802–1814 (2012).

40. Chen, G. *et al.* Regulation of FLC nuclear import by coordinated action of the NUP62-subcomplex and importin β SAD2. *J. Integr. Plant Biol.* **65**, 2086–2106 (2023).

41. Collins, P. P. *et al.* Characterisation of the trans-membrane nucleoporins GP210 and NDC1 in *Arabidopsis thaliana*. *Plant Sci.* **332**, 111719 (2023).

42. Tamura, K., Fukao, Y., Iwamoto, M., Haraguchi, T. & Hara-Nishimura, I. Identification and characterization of nuclear pore complex components in *Arabidopsis thaliana*. *Plant Cell* **22**, 4084–4097 (2010).

43. Mansfeld, J. *et al.* The conserved transmembrane nucleoporin NDC1 is required for nuclear pore complex assembly in vertebrate cells. *Mol. Cell* **22**, 93–103 (2006).

44. Blasius, T. L., Takao, D. & Verhey, K. J. NPHP proteins are binding partners of nucleoporins at the base of the primary cilium. *PLOS ONE* **14**, e0222924 (2019).

45. Craige, B. *et al.* CEP290 tethers flagellar transition zone microtubules to the membrane and regulates flagellar protein content. *J. Cell Biol.* **190**, 927–940 (2010).

46. Epting, D. *et al.* The ciliary transition zone protein TMEM218 synergistically interacts with the NPHP module and its reduced dosage leads to a wide range of syndromic ciliopathies. *Hum. Mol. Genet.* **31**, 2295–2306 (2022).

47. Li, C. *et al.* MKS5 and CEP290 dependent assembly pathway of the ciliary transition zone. *PLOS Biol.* **14**, e1002416 (2016).

48. Tang, Y., Huang, A. & Gu, Y. Global profiling of plant nuclear membrane proteome in Arabidopsis. *Nat. Plants* **6**, 838–847 (2020).

49. Arra, Y. *et al.* Rice Yellow Mottle Virus resistance by genome editing of the *Oryza sativa L. ssp. japonica* nucleoporin gene *OsCPR5.1* but not *OsCPR5.2*. *Plant Biotechnol. J.* **22**, 1299–1311 (2024).

50. Faulkner, C., Akman, O. E., Bell, K., Jeffree, C. & Oparka, K. Peeking into pit fields: a multiple twinning model of secondary plasmodesmata formation in tobacco. *Plant Cell* **20**, 1504–1518 (2008).

51. Fitzgibbon, J., Bell, K., King, E. & Oparka, K. Super-resolution imaging of plasmodesmata using three-dimensional structured illumination microscopy. *Plant Physiol.* **153**, 1453–63 (2010).